TEMPERATURE EFFECTS ON FINE-GRAINED SOIL ERODIBILITY

by

ABDULLAH MUBARAK ABDULMOHSEN AL-ALI

B.S., Kansas State University, 2013

A THESIS

submitted in partial fulfillment of the requirements for the degree

MASTER OF SCIENCE

Department of Civil Engineering
College of Engineering

KANSAS STATE UNIVERSITY
Manhattan, Kansas

2016

Approved by:

Major Professor
Dr. Tucker-Kulesza, Stacey E.

Copyright

Abstract

Recent climate changes may affect the stability of our infrastructure in many ways. This study investigated the effects of fine-grained soil temperature on erosion rate. If climate change is shown to affect the erodibility of soils the impacts must be identified to monitor the stability of existing infrastructure, improve design of levees and structures founded in erosive environments, and to prevent sediment loss and stream meanders. Fine-grained soil erosion is complicated by the dynamic linkage of multiple parameters, including physical, biological and geochemical properties. This study held constant all parameters that influence fine-grained soil erodibility while only varying soil temperature in order to study the effects it has on erodibility. This study also confirmed previous findings that water temperature affects soil erodibility. The main objective of this study was to investigate the effects of fine-grained soil temperature on erosion rate. This study also instrumented a turbidity sensor to reliably map soil erosion. Based on this research, the conclusion was made that an increase in soil temperature increases soil erosion rate. The turbidity sensor was a valuable tool for comparing soil erosion. Future studies should investigate the effects soil temperatures below room temperature, the magnitude of temperature increase or decrease, and the effects of cyclic heating and cooling on fine grained soil erodibility.

Table of Contents

List of Figures

List of Tables

Acknowledgements

I would like to acknowledge all that was there for me during my academic journey. First of all, I would like to direct my sincerest appreciation to my major professor Dr. Stacey E. Tucker-Kulesza for passing all the valuable knowledge onto me, adopting me as an academic son, and allowing me the opportunity to perform this study. I would also like to thank her for all the assistance, guidance, advice, and support she provided me with. In addition, I would like to express my gratefulness to my committee members Dr. David R. Steward, for being a role model in his academic achievements and Dr. Dunja Perić for introducing me to geotechnical engineering and molding me into the geotechnical engineer I am today.

I would also like to extend my gratitude to my family for all the support, and a special thank you to my brother Abdulmohsen Mubarak Abdulmohsen Al-Ali for sacrificing his summer vacation to assist me with the project. Thank you to all that made this research project possible, including Tamara Robinson for taking the time to edit this thesis. I would also like to acknowledge and thank all my colleagues, including Maryam Alhendi for all her help in preparing this thesis, Michael Snapp, Weston Koehn, and Md Zahidual for lending me a hand whenever needed.

Dedication

I, Abdullah Mubarak Abdulmohsen Al-Ali, dedicate my degree including the research project and this thesis to my wonderful family lead by my amazing parents, Mubarak Abdulmohsen Mubarak Al-Ali and Alyaa Abdulwahab Ali Almutawa in addition to my siblings Abdulwahab Mubarak Abdulmohsen Al-Ali, Shaikha Mubarak Abdulmohsen Al-Ali, Abdulmohsen Mubarak Abdulmohsen Al-Ali, and Najeeba Mubarak Abdulmohsen Al-Ali. Without all their continuous support and assistance I would not have achieved a fraction of what I have achieved today.

Chapter 1 - Introduction

Soil erosion is the leading cause of failure for bridges. In fact, approximately 58% of bridge collapses are attributed to scour (Briaud 2006). Fig. 1 shows scour developed around bridge pier. Soil erosion also causes levee failure, stream meander, and sediment loss, all of which reduce the natural capacity for flood control. Many factors contribute to the complex phenomenon of soil erosion, including soil properties, site geometry, vegetative cover, and hydraulic conditions. Although the hydrodynamic aspects of soil erosion and transport and erosion mechanisms of coarse-grained soils are well understood, the erodibility of fine-grained soils is difficult to predict and has been a challenge to many engineers. Fine-grained soil erosion must be understood to the same degree as coarse-grained soil. Continuation of poor estimations of fine-grained soil erodibility without a complete understanding of its erosion mechanisms is costly, and more importantly, places public safety in jeopardy.

Fig. 1 Scour developed around bridge pier (Johnson 2015)

Recorded temperatures on Earth have been rising dramatically in recent decades, whether it is a result of global warming or a natural cycle that Earth goes through. This climate change, which is anticipated to continue, is associated with less frequent but more extreme precipitation events (Trenberth 2011). While environmentalists are concerned with carbon dioxide concentrations and the impacts of high temperatures on the environment, civil engineers must address how environmental changes affect the infrastructure. For example, change in precipitation compounded with increasingly impermeable boundaries as the built environment expands will increase flooding and potentially cause additional damage to the existing infrastructure. Grabowski et al. (2011) identified temperature as a variable that affects fine-grained soil erosion, so this study investigated the effects of increasing soil temperatures on its erosion rate. Investigating the effects of temperature on fine-grained soil erosion rate contributes to fundamental knowledge of the mechanisms of fine-grained soil erosion and perhaps contributes to a more complete understanding of it.

Prior to this study, effects of soil temperature on fine-grained soil erosion were unknown. Although Grabowski et al. (2011) identified temperature as a variable that affects erosion, previous researchers studied the effects of water temperature, not soil. For example, Larionov (2014) showed that an increase in water temperature results in increased erosion. This study demonstrated that varying soil temperatures have profound effects on fine-grained soil erodibility. Based on results of this study, researchers conducting future erosion laboratory tests on undisturbed samples should measure the in situ soil and water temperatures and conduct experiments at temperatures representing in situ conditions. Furthermore, results suggested that a flooding event of a certain

magnitude in cold seasons would result in a less severe outcome than a flood event of the same magnitude in warm seasons.

The Erosion Function Apparatus (EFA) measures the erosion rate of undisturbed soil samples obtained from the field for a given flow velocity of water (Briaud et al. 1999, 2001, 2004). The EFA can be used in conjunction with SRICOS (Scour Rate in COhesive Soils) method to estimate scour on and around bridge piers founded in cohesive sediment (Briaud 2006). Erosion rate obtained from the EFA as a function of shear stress or flow velocity may be used to classify soil erodibility by measuring the soil erosion function. Although numerous laboratory devices measure scour rate, the EFA was exclusively used in this study. Detailed information regarding other laboratory and in situ testing devices are stated in Chapter 2.

The EFA at Kansas State University (KSU-EFA) is distinct from other EFAs due to the addition of a turbidity sensor. Instrumenting the KSU-EFA with the turbidity sensor was included in this study. A turbidity sensor operates by measuring the scattering of light in a liquid media at a 90 ° angle from the light source. The sensor was employed in this study to measure water clarity downstream from erosion occurrences in order to quantify erosion as soil particles circulate through the system.

Fine-grained soil erosion is complicated due to dynamically linked geochemical, biological, and physical properties (Grabowski et al. 2011). Geochemical properties include clay mineralogy, total salinity, cations (sodium adsorption ratio), pH levels, metals, and organic content. Biological properties include sediment disturbance, feeding and egestion, and biogenic structures. Physical properties include mean particle size, particle size distribution, bulk density, water content, and temperature. This study held all

properties constant while varying only soil temperature in order to determine the impact of soil temperature on erodibility.

A custom heating system was developed to increase the temperature of soil samples. The system utilized a heating jacket, thermocouples, and a data acquisition system. The heating jacket was wrapped around a Shelby tube that contained the soil sample. Thermocouples protruded into the bottom of the sample to monitor soil temperature, and the data acquisition system collected and stored data. Fig. 2 shows a schematic of the heating system.

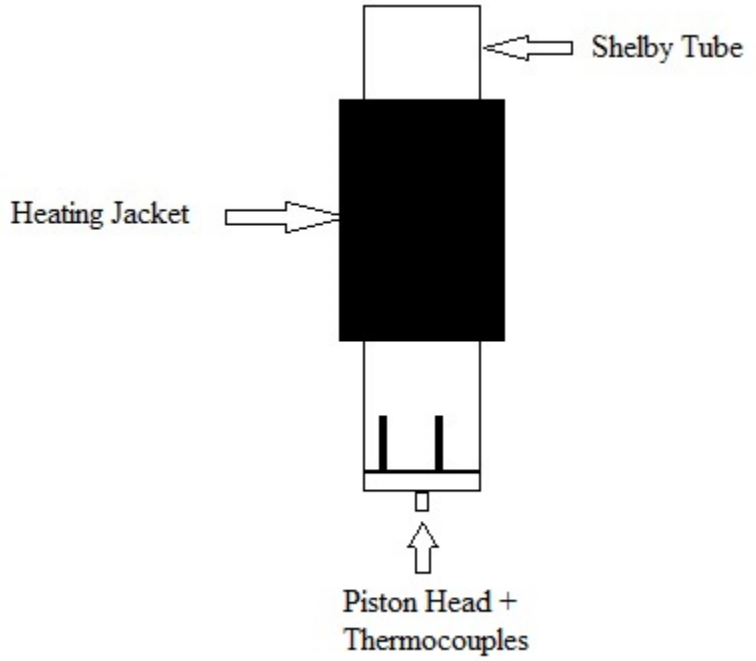

Fig. 2 Schematic of the heating system

All samples were 100% kaolin clay mixed at the same water content and compactive effort so that effects of temperature could be studied individually. In order to ensure preparation of identical samples, samples were tested in the EFA at identical water

velocity to confirm identical erodibility. All samples were compacted in a Shelby tube to the maximum dry unit weight at optimum water content determined by the Standard Proctor test, 14.23 kN/m^3 ± 1 kN/m^3 and 29%, respectively. Additional details regarding sample preparation are outlined in Chapter 3. Table 1 shows results of samples tested to confirm consistent erosion rates before varying soil temperature. Samples C and D were tested multiple times to confirm consistent results within a sample. The most extreme difference in erodibility between samples was 3 mm/hour, occurring at a velocity of 4 m/s, which was deemed reasonable for the purposes of this study.

Table 1 Preliminary room temperature samples results

Sample ID	Dry Unit Weight (kN/m^3)	Water Content (%)	3 m/s (mm/hr)	4 m/s (mm/hr)	5 m/s (mm/hr)	6 m/s (mm/hr)
A	14.66	29	4	10	NA	NA
B	14.80	29.5	4	9	11	14
C	14.70	29.3	5	10	11	13
C-1	14.70	29.3	4	9	11	14
C-2	14.70	29.3	4	8	NA	NA
D	14.74	29	4	7	NA	NA
D-1	14.74	29	3	7	NA	NA

No known method exists to appropriately predict erodibility of fine-grained soils. Existing methods are over conservative or require specialized, costly testing. Fine-grained soil erosion must be predicted with the same accuracy as coarse-grained soils, but this cannot be done until researchers understand the fundamental mechanism that causes fine-grained soils to erode. Temperature has been identified as one of the variables that affects soil erodibility.

The main objective of this study was to investigate the effects of soil temperature on fine-grained soil erosion. In an EFA test, an operator typically visually observes erosion and reports the amount of erosion. However, this method is user dependent since each user has unique judgments as to how much soil has eroded. Therefore, an additional

objective was to instrument the EFA with a turbidity sensor to reliably map soil erosion. This will help more accurately compare results obtained by different users regardless of their method of judgment. Because a standard EFA test requires about 8 hours of sample testing and monitoring, the third objective of this study was to shorten the test duration.

This thesis is organized in the following manner. Chapter 2 contains a literature review that includes discussion of factors affecting fine-grained soil erosion and an overview on in situ and laboratory testing devices. Chapter 3 describes methodology used for sample preparation, sample testing, and sample heating in this study. Chapter 4 presents findings of this study, and Chapter 5 includes conclusions and suggestions for future work.

Chapter 2 - Literature Review

Erosion

Soil erodibility is defined as mobility of soil particles due to high winds or flowing water. This research, however, focused on soil particle mobilization due to flowing water (i.e., scour). Understanding and quantifying soil erosion is critical to improve structures' design to withstand erosive environments. Erosion impacts infrastructures, such as bridge foundations and levees, as well as natural environments, including sediment loss and stream meander. The mechanism of soil erosion varies greatly between fine-grained soils and coarse-grained soils. Some fine-grained soils, such as clay, tend to erode in clumps of particles due to the presence of attractive forces between particles, or cohesion, which makes its erodibility very complex and unpredictable. However, coarse-grained soils erode particle by particle, making its erosion possible to model. The coarse-grained soil erosion mechanism is likely due to the absence of attractive forces between particles. Following this introduction, this chapter includes a discussion of fine-grained and coarse-grained soil erosion, a description of field and laboratory testing devices, and erosion mapping from utilization of sensors.

Fine-Grained Soil Erosion

An extensive review by Grabowski et al. (2011) revealed that despite all the efforts to understand and predict fine-grained soil erosion, it remains complicated. Such complexity is attributed to the dynamically linked interaction between biological, geochemical, and physical soil properties shown in Fig. 3. Fine-grained soils are composed of organic and inorganic solids, water, and gasses (Gebert et al. 2006; Sanders et al. 2007). Electrochemical activity, predominantly in clays, is the interaction between electrically charged clay particles with

surrounding media, such as water. This interaction results in the formation of a coating over the particles known as a double layer, which is also known to influence erodibility (Gerbersdorf et al. 2007). By varying any of the properties illustrated in Fig. 3, where the fine-grained soil exists, will affect its erodibility due to complex soil property interactions (Grabowski et al. 2011). Soil erosion occurs when erosive forces such as shear stress and turbulence induced by water flow (Leeder 1999) and transportation of particles along the sediments surface (Amos et al. 1998), overcome the resistive forces, which include gravity, friction, cohesion, and adhesion (Winterwerp and van Kesteren 2004). When considering rivers and sediment transport specifically, the conditions under which sediments settle to form a bed have an impact on its erodibility as well. Studies have shown that when sediment settles while exposed to shear stress, it tends to be more stable and less susceptible to erosion, compared to sediment that settle under no shear stress, this is because sediment that settles under shear stress is larger in particle size and denser, requiring a greater force to mobilize it (Grabowski et al. 2011).

Erosion is initiated when the shear stress imposed is equal to or greater than critical shear stress; erosion does not occur at shear stresses lower than critical shear stress. Critical shear stress is related to critical velocity, where critical velocity is the flow velocity required to generate critical shear stress. The velocity required to achieve critical shear stress depends on characteristics of the eroding fluid. In this study, characteristics of the eroding fluid were held constant. Partheniades (1965) showed that erosion rate can be estimated by the following expression:

$$E = M(\tau_c - \tau_b), \qquad \textbf{Eq 1}$$

where E is erosion rate, τ_b is bed shear stress, τ_c is critical shear stress, and M is a material-specific constant.

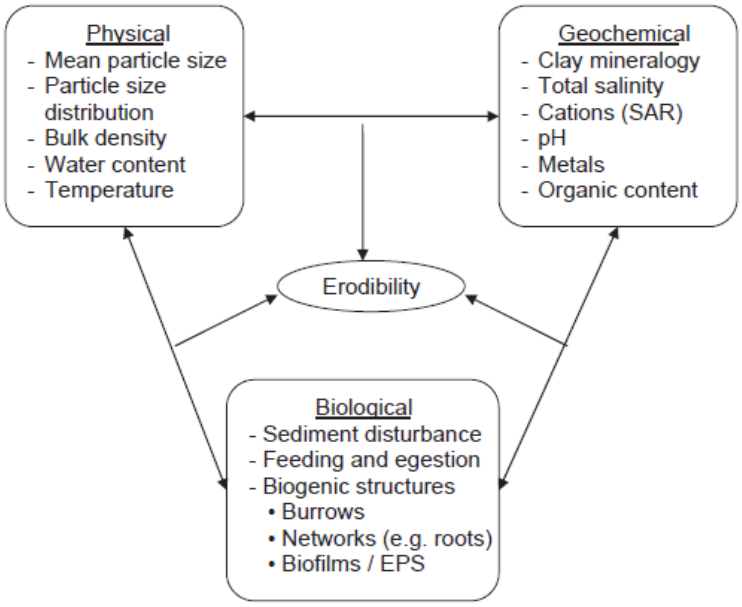

Fig. 3. Sediment properties and processes that affect sediment erodibility (Grabowski et al. 2011)

Geotechnical engineers are typically interested in physical properties of soils and how they affect soil erodibility. Jepsen et al. (1997) investigated the effects of varying bulk density, water content, and compaction on erosion rates. Jepsen et al. (1997) collected soil samples from three sites and reconstructed them in coring tubes to allow increased control over their bulk densities. Composition and location of each sample were as follows: quartz, muscovite, dolomite, and calcite from the Detroit River in Michigan; quartz, albite, dolomite, illite, and kaolinite from the Fox River in Wisconsin; and albite, quartz, and microcline from a slough near Santa Barbara, California. A mixture of water and sediment were poured in coring tubes at various depths and allowed to consolidate under their own weight over various time intervals to produce unique bulk densities. Results from the Jepsen et al. (1997) study revealed an inverse relationship between erosion rates and bulk density. As bulk density of a fine-grained soil

increases, the erosion rate decreases significantly. Fig. 4 illustrates the decrease in erosion rates with an increase in bulk density at shear stresses of 2, 4, 8, 16, 32, and 64 dynes/cm^2 for the sample obtained from Fox River. Note that a dyne is a unit of force equating to 10 μN.

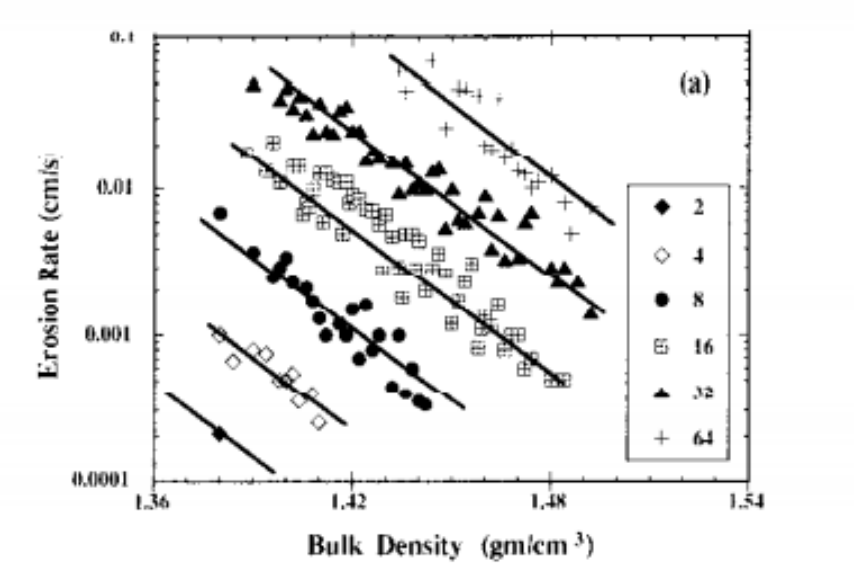

Fig. 4. Erosion rate as a function of bulk density (Jepsen et al. 1997)

Although studies have shown that soil erodibility depends on multiple soil properties, this research focused only on physical soil properties since biological and geochemical soil properties are held constant. Samples used in this study were composed of manufactured kaolin clay with particle size distribution ranging from a minimum of 0.00029 to 0.028 mm. In this study, the effects of varying internal temperatures of soil samples were investigated, where samples were heated using a heating jacket wrapped around a Shelby tube containing the soil sample. Traditionally the temperature of the circulating water increased as the water circulated through the system, and kinetic energy was converted to thermal energy. Larionov et al. (2014) investigated the effects of water temperature and soil moisture content on the erodibility of heavy loamy chernozemic (loess-like loams) soil samples using a downward vertical jet of water.

Results showed that samples eroded more when tested with warmer water. Larionov et al. (2014) hypothesized that this finding was a result of electrostatic forces and not hydraulic forces since warm water is less viscous than cold water, yielding less erosion. Water temperatures were tested at 0, 5, 10, 15, 20, and 25 ˚C. Fig. 5 shows a plot of temperature versus erodibility, demonstrating that erodibility increases as an exponential function. In this study, water temperatures were allowed to increase gradually over the duration of the test, from 16 to 30 °C, rather than maintaining a constant temperature throughout the test.

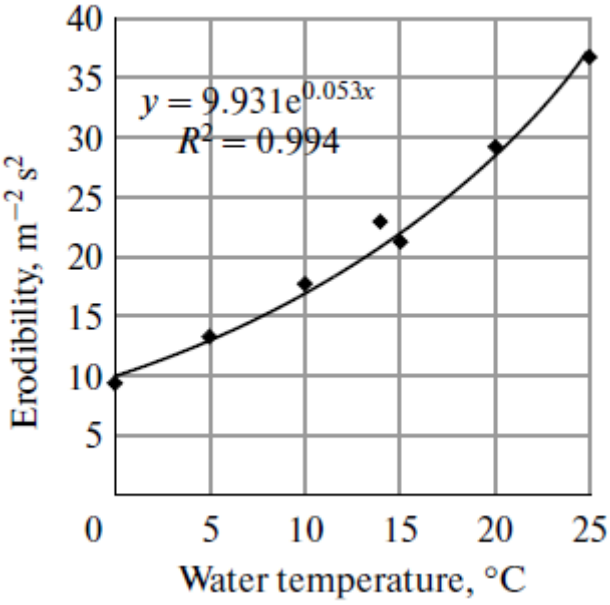

Fig. 5 Water temperature effects on erodibility (Larionov et al. 2014)

Larionov et al. (2014) also demonstrated the influence of water content on soil erodibility. Soil samples were tested at 16%, 18%, 20%, 22%, 24%, 26%, 28%, and 30% water content. Results showed that erodibility decreases as water content increases up to 24%, after which erodibility began to increase, resulting in the parabolic shape in Fig. 7. Larionov et al. (2014) defined 20 °C to be the standard temperature at which soil samples should be studied.

Inbar et al. (2014) studied the effects of forest fires on erosion rate due to surface runoff. Soil samples were obtained from areas directly exposed to fire, and from an adjacent area not exposed to fire. Some of the unburned soil was heated to 300 °C in a muffle. The various soil samples, directly exposed to fire, heated, and unburned, were tested in the laboratory using rainfall simulator where, runoff, soil loss and infiltration rates were measured. The soil obtained from the forest is composed of sandy clay loam. Runoff and soil loss amounts were lowest, intermediate, and highest in the heated, direct fire, and unburned soils, respectively. The soil samples were subjected to three rainstorm events and results shown in Fig. 6 indicate that the unburned soil, soil loss was greater in the second rainstorm event than in the first rainstorm event and then decreased in the third rainstorm event, this resulted in the most soil loss in the first and second rainstorm events across all three soil samples tested. Soil loss in the soil sample that was exposed to direct fire increased after each consecutive rainstorm event causing the amount of soil loss to exceed that of the unburned soil in the third rainstorm event. As for the soil that was heated to 300 °C, soil loss increased after each consecutive rainfall event, nevertheless, amounting in the least soil loss out of all soil samples tested.

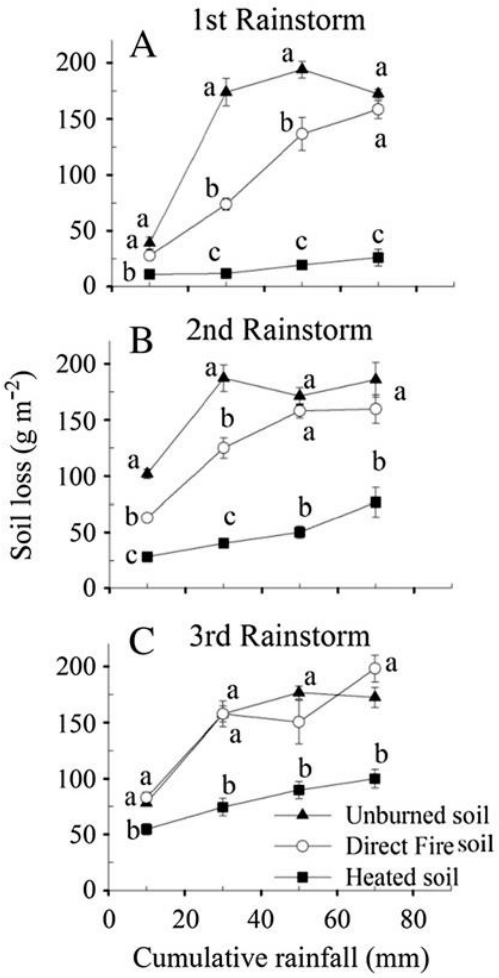

Fig. 6 Soil loss results for three rainstorm events (Inbar et al. 2014).

The exposure to extreme heats and open flame alters the chemical, physiochemical and physical properties of the soil. In this study, however, the soil was heated to temperatures between 30 and 37 °C.

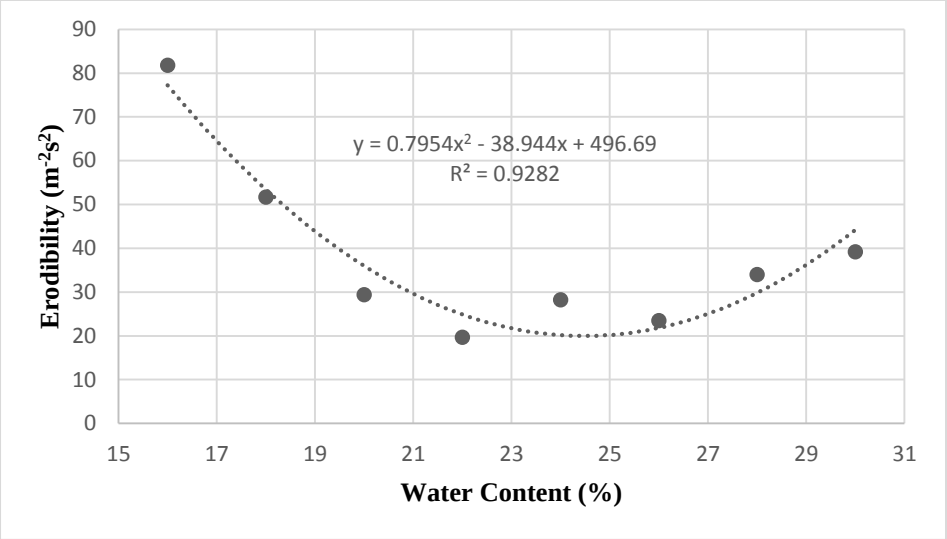

Fig. 7 Water content effects on erodibility (adapted from Larionov et al. 2014)

Coarse-Grained Soil Erosion

The manner in which coarse-grained soils erode varies greatly from that of fine-grained soils. Due to lack of interparticle attractive forces, coarse-grained soils typically erode particle by particle rather than in clumps. Roberts et al. (1998) investigated the effects of particle size and bulk density on the erosion rates of quartz particles. Results showed that as particle size increased, the erosion rate also increased up to a maximum particle size, after which the erosion rate began to decrease. The quartz particles had mean diameters of 5.7, 14.8, 18.3, 48, 75, 125, 222, 432, 1,020, and 1,350 μm. Results are shown in Fig. 8 (a), (b), and (c) at bulk densities of 1.65, 1.85, and 1.95 g/cm^3, respectively, exposed to shear stresses of 0.2, 0.4, 0.6, 0.8, 1.6, and 3.2 N/m^2. The decrease in erosion rates was assumed to be due to the increased weight of particles larger than 100 μm. Sediments containing particles larger than 48 μm consolidated at an accelerated rate, resulting in high bulk densities; therefore, bulk density of 1.65 g/cm^3 was not achievable.

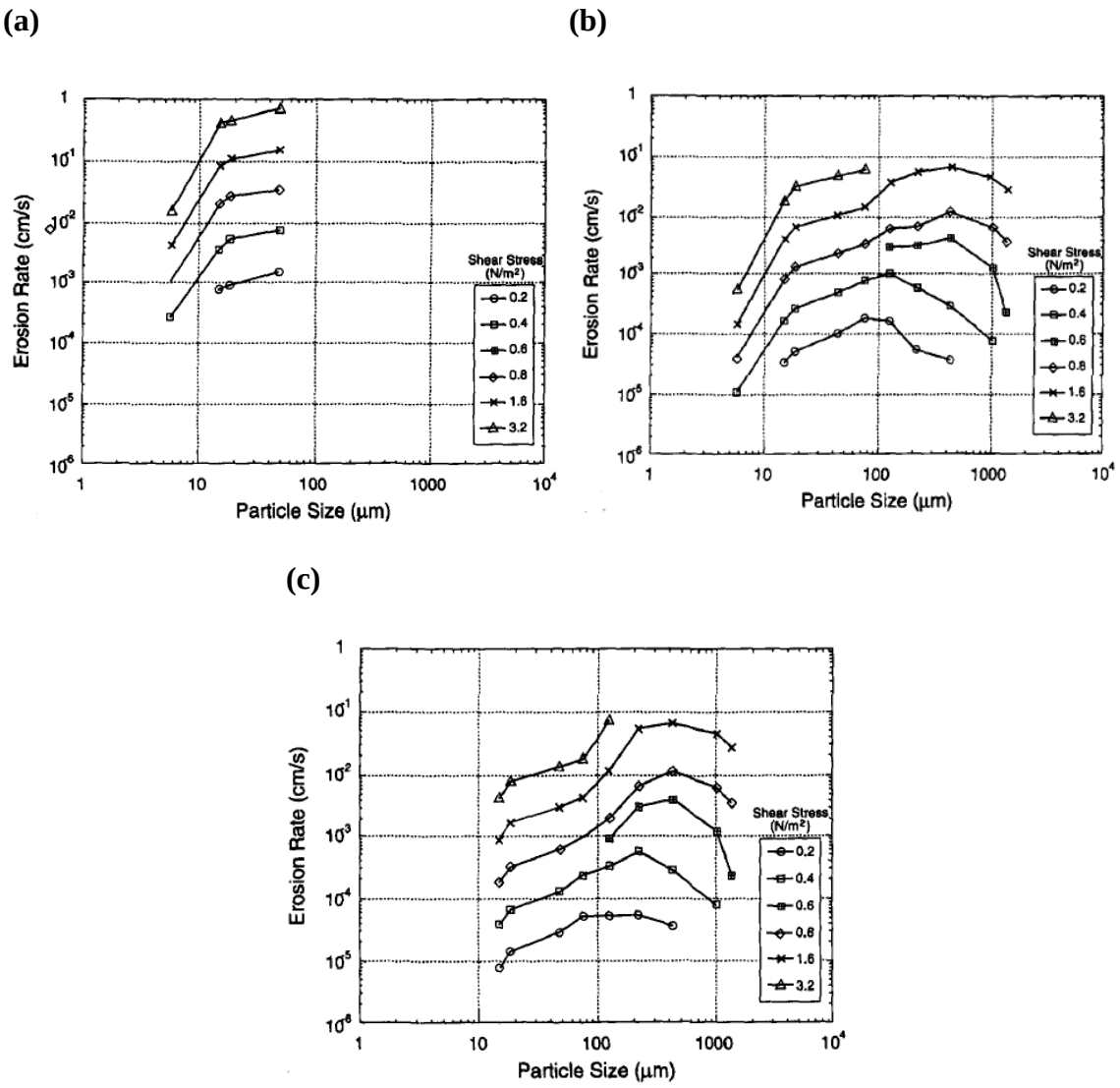

Fig. 8. Erosion rate as functions of particle size for bulk densities of (a) 1.65, (b) 1.85, and (c) 1.95 g/cm^3 (Roberts et al. 1998)

Roberts et al. (1998) also found that samples made from quartz particles at least 1,350 μm in size varying the bulk density had no impact on erosion rate. Nevertheless, an inverse relationship was observed between small quartz particle size erosion rates and bulk densities. Fig. 9 (a) and (b) show erosion rates as functions of bulk densities for particle sizes of 14.8 and 75 μm, respectively. A noticeable trend of decreasing erosion rates occurred as bulk density

increased for shear stresses of 0.2, 0.4, 0.6, 0.8, 1.6, and 3.2 N/m^2. Fig. 9 (c), however, shows no change in erosion rates as bulk density increases for particle size of 1,350 µm.

Although demonstration of the effects of varying particle sizes and bulk densities was worthy, this study focused only on fine-grained soils, specifically manufactured kaolin clay. Manufactured kaolin clay was chosen because it was readily available in the laboratory, it demonstrates ease of sample preparation, and it is commonly used for reconstituted samples.

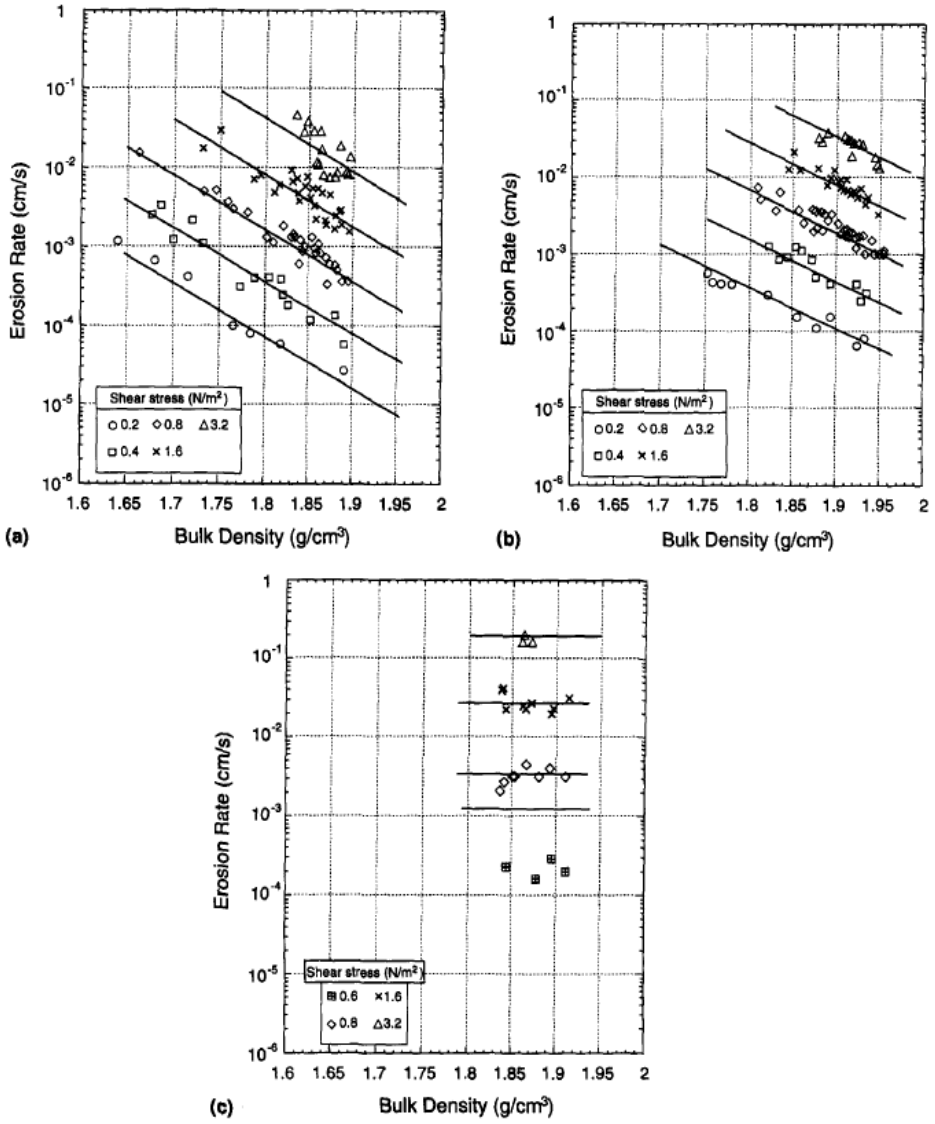

Fig. 9. Erosion rates as functions of bulk density at various shear stresses (a) particle size 14.8 µm, (b) particle size 75 µm, and (c) particle size 1,350 µm (Roberts et al. 1998)

Field Erosion Testing

Over the past decades, many soil erosion devices were developed to measure soil erosion rates in situ as well as in the laboratory. Erosion rates have been reported as mass per time or distance per time, with the distance referring to thickness of sediment eroded. All devices, mentioned thereafter, are similar in the way they evoke erosion by making use of a fluid media to transfer shear stresses over the sediment in question. Each device has advantages and disadvantages which are discussed herein. In this study, the Erosion Function Apparatus (EFA), was used exclusively. Because erosion rates are unique to each device, erosion rates obtained from different devices cannot be compared with one another, therefore it is critical that only one device be used to study how one parameter alone influences erodibility.

FLUME

FLUME is an apparatus that measures in situ rate of erosion of sediment. Ravens (2007) describes FLUME as a 3 m long, straight flume with cross-sectional dimensions of 10.1 x 12.7 cm. A horizontal bar is contained in the first half of the FLUME, which expedites the development of a hydrodynamically fully developed flow. Following the flow development section is a 1.1 m long test section, where flowing water is brought into contact with the surface of the sediment to be tested. Fine sand was glued to the bottom of the FLUME's inlet in order to minimize the change in roughness as flow passed to the test section. A paddlewheel flow sensor was used to monitor the flow rate. In order to quantify the concentration of mobilized particles, a turbidimeter was employed and a calibration curve utilized, relating concentration of sediment in suspension to turbidity, where turbidity was recorded every 15 seconds. A diagram of FLUME is shown in Fig. 10.

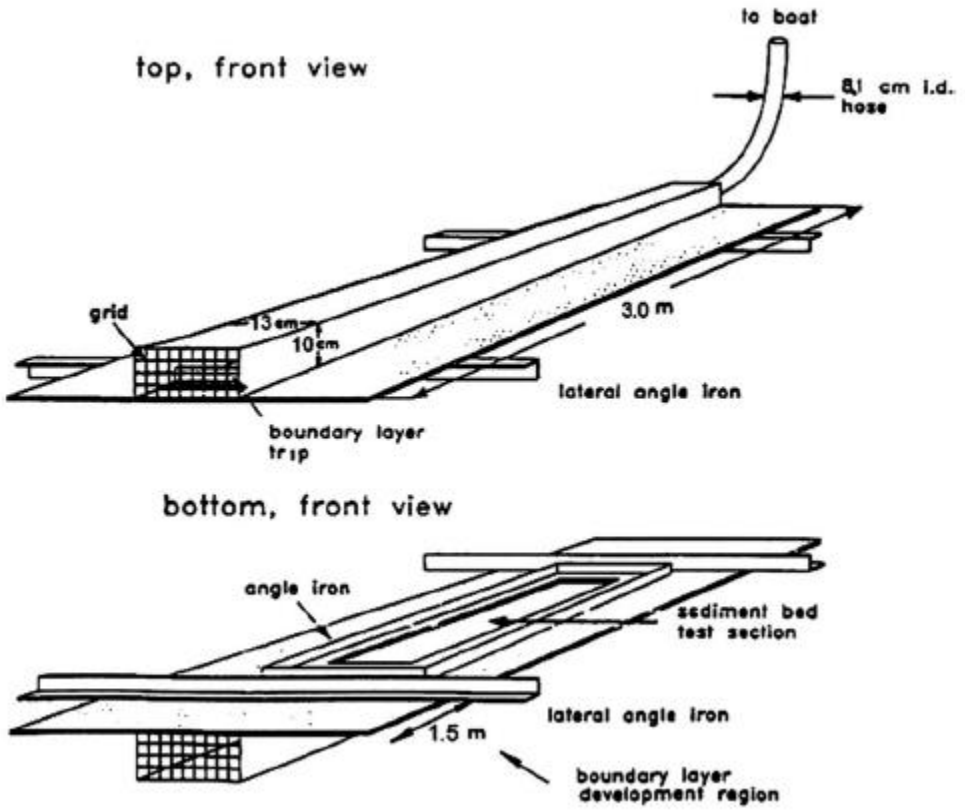

Fig. 10. Diagram of FLUME (Ravens 2007)

Ravens (2007) stated that the FLUME was deployed in situ from a boat using an onboard winch system and assistance from a scuba diver. An advantage of the FLUME is that it can be deployed directly on the surface of sediment in question without sampling. One disadvantage of the FLUME is that as flow rate increases, more erosion is induced and, consequently, the cross-sectional area of the test section varies, further reducing the flow velocity in addition to lower imposed shear stresses. Another consequence of the varying cross-sectional area is that when erosion depth exceeds 4 cm, scour pits may develop at the entrance and exit of the test conduit. When engaging FLUME, changes in effective cross-sectional area of the test conduit must be accounted for. In the FLUME erosion rates are reported as mass per area per time. FLUME is categorized as open channel flow erosion. By knowing average flow velocity, *U*, and fluid

density, ρ, Ravens (2007) demonstrated that the applied shear stress could be calculated by utilizing the following expression:

$$\tau = \rho \frac{f}{8} U^2, \qquad \textbf{Eq 2}$$

where τ is applied shear stress and f is friction factor. The friction factor can be calculated using the Colebrook formula (Munson et al. 2002)

$$\frac{1}{\sqrt{f}} = -0.869 \ln\left(\frac{\varepsilon / \mathrm{D}}{3.7} + \frac{2.51}{\mathrm{Re}\sqrt{f}} \right), \qquad \textbf{Eq 3}$$

where ε is roughness length, D is hydraulic diameter, and Re is Reynolds number. The Reynolds number can be obtained through the following equation:

$$\mathrm{Re} = \frac{UD}{\nu}, \qquad \textbf{Eq 4}$$

where ν is kinematic viscosity and all other variables have previously been defined.

Jet Erosion Testing

Hanson and Cook (2004) developed an erosion testing device, the Jet Erosion Testing (JET) apparatus, used in situ to characterize soil erodiblity. Advantages of JET include its simplicity to carry out a test, speed with which tests can be conducted, and inexpensive performance. JET is preferable when the soil in question is a native streambed material to reduce sample disturbance. One disadvantage of JET is its inability to directly measure and control shear stress. Another disadvantage is that, as scour develops, the distance between the nozzle and the soil surface changes continuously, affecting the stresses imposed at the sediment surface.

The JET apparatus is comprised of a 0.92 m long jet tube, a nozzle with a diameter of 6.4 mm, an air relief valve, a point gauge, an adjustable head tank, and a jet submergence tank. The adjustable head tank is made up of 0.91 m clear tubing to allow visual surveillance of the water level. The air relief valve is used to relief air pressure that may accumulate in the jet tube during filling. Because the point gauge is aligned with the nozzle, measurement of scour can be taken as flow is stopped by the point gauge that has a diameter equal to the diameter of the nozzle. The steel submergence tank is 0.3 m in diameter and height with a tube frame attached to secure the jet tube at the center of the tank. The submergence tank is open on both ends; when the tank is driven into the soil, a seal is formed at the bottom of the tank, allowing the tank to be filled with water. Erosion rate is reported as volume per time. A schematic of the submersible JET apparatus is given in Fig. 11.

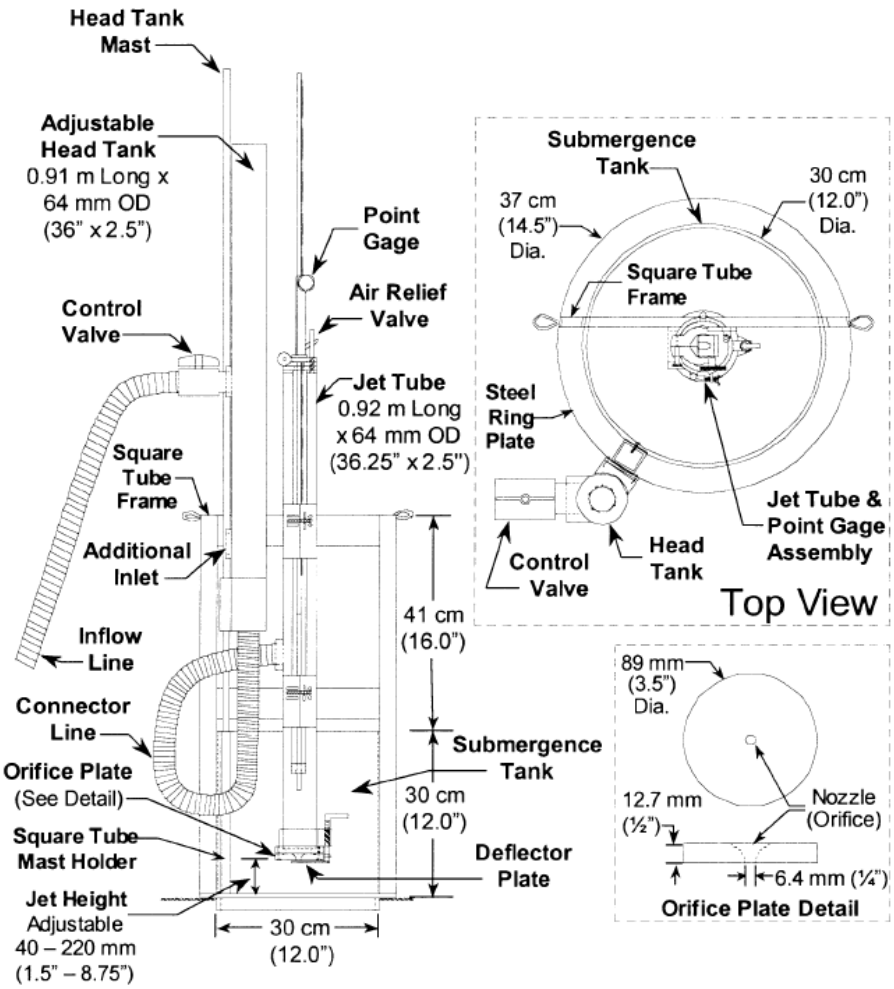

Fig. 11. Schematic of JET (Hanson and Cook 2004)

A jet index was developed to characterize erosion resistance of soils as empirically related to soil erodibility (Hanson 1991). ASTM designation D5852 can be referred to for detailed testing apparatus and method for determining the jet index. Hanson and Cook (2004) recommended that the JET nozzle should be 12 nozzle diameters above the sediment's surface before initiating a test. A set of 10–12 point gauge readings of the sediment bed was recorded, allowing 5–10 minutes between readings to determine depth of scour.

Laboratory Erosion Testing Techniques

Erosion tests conducted in laboratories can be done using any of the devices mentioned in this section. All devices have the ability to test undisturbed or reconstituted soil samples. In this section the device used in this study, the EFA, is described, followed by a brief description on the Rotating Erosion Testing Apparatus (RETA). Next, four other flume style devices which include: Sediment Erosion Rate Flume (SERF), Sediment Erosion at Depth Flume (SEDFlume), Adjustable Shear Stress Erosion and Transport (ASSET), and Recirculating Flume, are discussed.

Erosion Function Apparatus

The EFA (Briaud et al. 2001) test section is a rectangular pipe with internal cross-sectional dimensions of 101.6 mm x 50.8 mm and a length of 1.22 m. The rectangular conduit is equipped with a flow straightener situated in the upstream end of the conduit. The apparatus is equipped with a pump to drive flow through the test section and back to the water reservoir located at the rear end. The presence of a valve allows flow regulation; velocities up to 6 m/s are achievable. A thin-walled Shelby tube sampler is mounted over a motor-controlled piston, with one end of the Shelby tube held flush with the flume's bottom through a circular cut in the test section. The piston pushes the sample through the Shelby tube so that its surface remains flush with the bottom of the flume as water flows over it. In addition to a flow meter, a thermometer is fixed downstream from the test section in order to measure the flow rate and temperature, respectively. Circular PVC pipes are used to guide the flow from the reservoir to the test section and back to the reservoir. Erosion rates are given as the distance the piston travels upwards per time. Fig. 12 shows a conceptual diagram of the EFA's test section.

A standard test determines the erosion rate versus shear stress and erosion rate versus velocity by testing the soil sample at six water flow velocities. Each velocity circulates for 1 hour, and the amount of erosion is recorded. The samples' surfaces is maintained flush with the flume's bottom at all times during the test. An operator monitors the test and extrudes the sample into the flume as soon as the top layers eroded.

Modifications were made to the EFA in this study; a turbidity sensor was instrumented downstream from the test section in order to map erosion. Additional modifications were made to the flume in order to accommodate tubes of various diameters. Initially the flume could house only Shelby tubes that were 76.2 mm in diameter and greater than 609.6 mm in length. Currently the flume is capable of housing Shelby tubes that are 76.2 and 88.9 mm in diameter and as short as 152.4 mm in length.

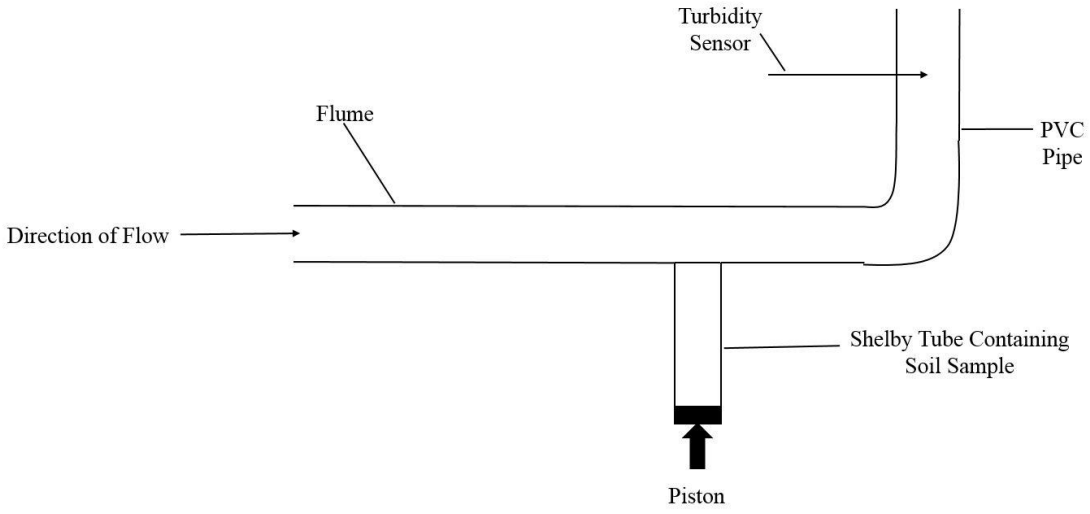

Fig. 12. EFA's test section

The EFA was originally designed to predict scour susceptibility. Briaud (2004) developed Scour Rate In COhesive Soils Erosion Function Apparatus (SRICOS-EFA) to predict scour depths versus time curve in fine-grained soils. The SRICOS method requires the following steps:

1. Obtain a sample in a standard 76.2 mm Shelby tube.
2. Perform a standard EFA test to obtain erosion rate versus shear stress curve.
3. Determine the maximum shear stress present on the river bed at the beginning of the scour process.
4. Obtain an initial scour rate corresponding to maximum shear stress in Step 3.
5. Calculate the maximum depth of scour.
6. Develop the complete scour depth versus time curve.
7. Predict the depth of erosion by reading the curve from Step 6 at the time corresponding to the duration of the flood.

Eq 2, Eq 3, and Eq 4 are used to calculate shear stress, friction factor, and Reynolds number, respectively. The erosion rate, $\dot{z}$, is

$$\dot{z} = \frac{h}{t}, \qquad \textbf{Eq 5}$$

where h is the length of sample eroded and t is time.

A standard EFA test was conducted on the kaolin clay used in this study. The result of the standard test is shown in Table 2. The slightly shorter duration of the test at a velocity of 4 m/s was taken into account when necessary calculations were performed to obtain the erodibility plot shown in Fig. 13.

Table 2 Results of a standard EFA test

Flow Velocity (m/s)	Time (s)	Distance Eroded (mm)	Erosion Rate(mm/hour)
1	3600	1.00	1.00
2	3600	2.50	2.50
3	3600	6.00	6.00
4	3090	7.00	8.16
5	3600	12.00	12.00
6	3600	15.00	15.00

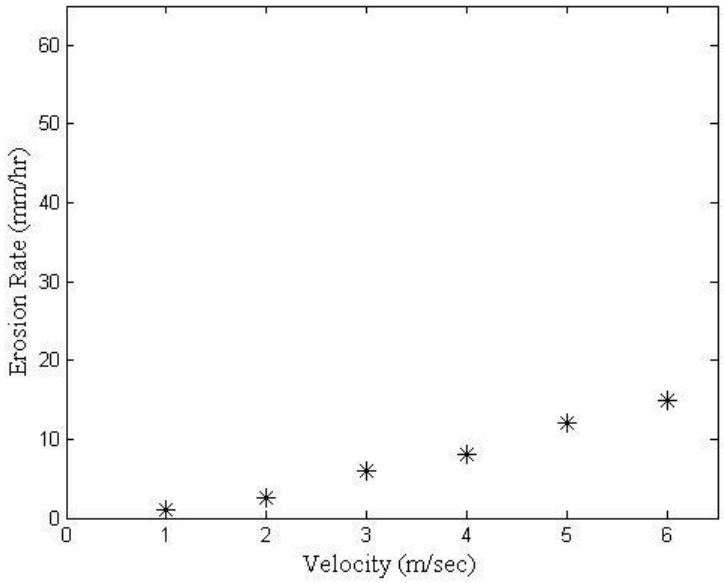

Fig. 13 Erodibility curve of a standard EFA test

Briaud (2008) proposed six erosion categories to classify soil and rock erodibility based on erosion rate at a given velocity or shear stress. The proposed categories ranged from very high erodibility to non-erosive. Fig. 14 and Fig. 15 represent the erosion categories based on velocity and shear stress, respectively. The kaolin clay used in this study reconstituted as described in Chapter 3 - classifies as medium erodibility.

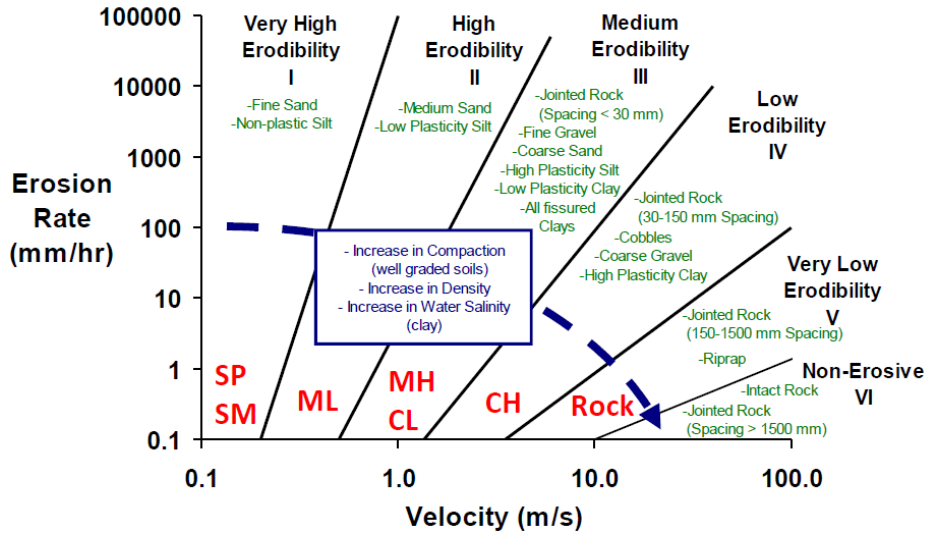

Fig. 14 Erodibility classification based on velocity (Briaud 2008)

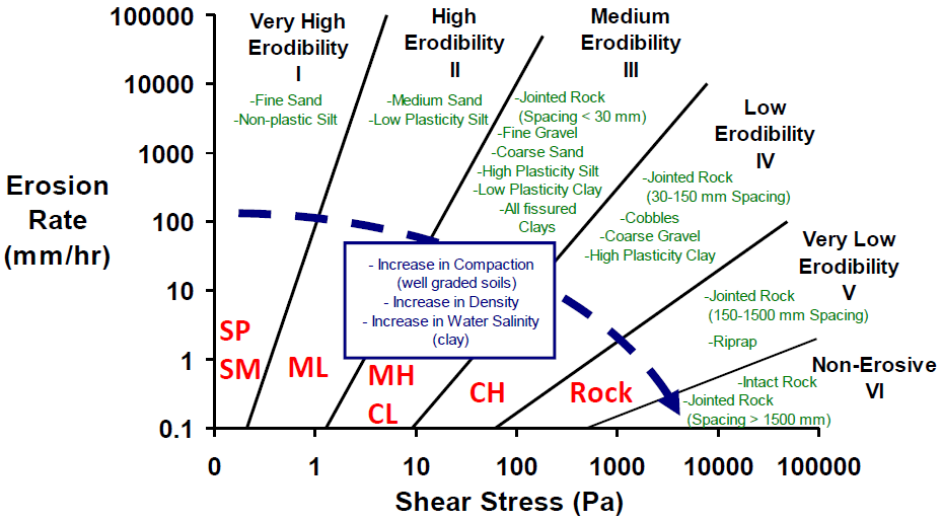

Fig. 15 Erodibility classification based on shear stress (Briaud 2008)

The EFA is advantageous because when used in conjunction with SRICOS method the scour potential around bridge piers can be estimated. Also, it is able to measure erodibility at a specific flow velocity, it is able to monitor the circulating fluid's temperature, and it can test undisturbed field samples. The main disadvantage of the EFA is its inherent dependence on operator's judgment to determine the extent of erosion in order to extrude the sample an equal

amount for the sample's surface to remain flush with the flume's bottom. In addition, EFA is unable to measure and control shear stress and pressure in the flume from the flowing water, a standard test requires at least eight hours, and as the sample erodes it affects the water clarity, making it harder and sometimes impossible to observe the sample through the glass window. The EFA device is also unable to maintain a constant temperature of circulating fluid throughout the test, though this is currently being resolved.

Due to the limitations of the standard Humboldt EFA, part of this study involved adapting the standard as built Humboldt EFA to address some of the limitations. Instrumentation of a turbidity sensor was deemed necessary to map erosion, to obtain a measurement of erosion when the water was too murky to see through the window, and to aid in shortening the testing period. In addition to the turbidity sensor, alterations to the flume's opening were performed to accommodate various diameters of Shelby tubes, commonly used by Kansas Department of Transportation and the Army Corps of Engineers, and an adjustable platform was added to accommodate shorter Shelby tubes. Current modifications include a pump motor control to eliminate overheating the water, a cooling system to maintain constant water temperature throughout the test, and a digital photogrammetry routine to measure the soil surface roughness.

Rotating Erosion Testing Apparatus

Shear stress induced by the flow of water is the leading mechanism responsible for erosion. The Rotating Erosion Testing Apparatus (RETA) was developed to increase understanding of how the magnitude of shear stress is associated with erosion rates (Crowley et al. 2012a). RETA, originally developed by Moore and Masch (1962), houses a cylindrical cohesive sediment, 76.2 mm diameter and length, and is capable of achieving rotational speeds of up to 2500 rpm. RETA is compact in size compared to other laboratory devices, it includes an

outer cylinder surrounding the sample. The annulus between the centered sample and the outer cylinder is filled with a fluid that induces shear stress on the sample as the outer cylinder rotates. Originally tests filled the annulus with a mixture of glycerin and water. Later it was discovered that glycerin had an impact on sediments' erodibility, making it more resistive to erosion. Therefore, only water was used as the shear-producing fluid, with a reduction in annular space and an increase in rotational velocity to compensate for the less-viscous fluid.

A later version of RETA (Crowley et al. 2012a; Sheppard and Bloomquist 2005) was described as a rotational style device, which operates by placing a 101.6 mm long cylindrical soil sample at the center of a rotating outer cylinder. When the annulus is filled with water it induces shear stresses on the centered sample. The samples were either 60.96 mm or 101.6 mm in diameter. In addition to the rotating outer cylinder, the device includes a motor and a torque cell-clutch that work together to control the rotational speed in real time, such that the induced average shear stress remains constant throughout the test. A 6.35 mm diameter hole was axially drilled through the sample, where one end of the support shaft was to be attached. The other end of the shaft was connected to a torque measuring load cell. A schematic of RETA is shown in Fig. 16.

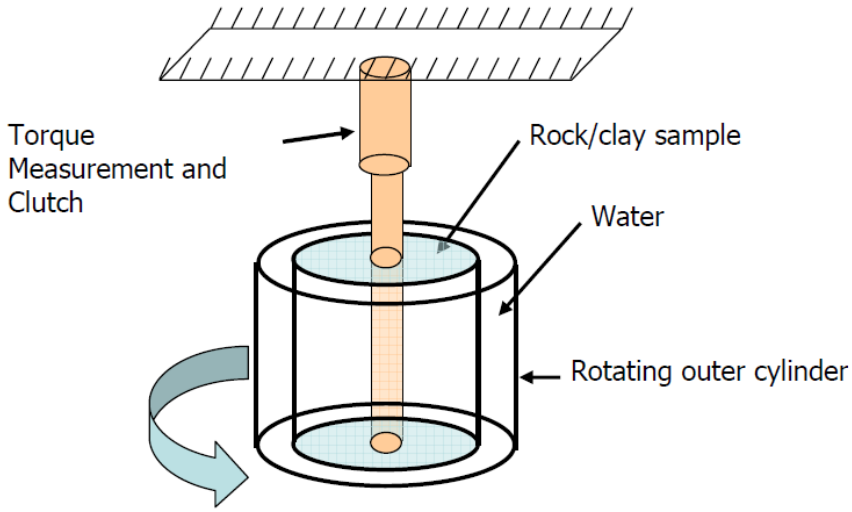

Fig. 16. Schematic of RETA (Sheppard and Bloomquist 2005)

In RETA, erosion rate is determined by measuring the mass of eroded soil, separating the solid particles from water present in the annulus, resulting in the mass of eroded solids. Units of erosion rates determined by weighing the mass of eroded particles are mass per time (Crowley et al. 2012a; Sheppard and Bloomquist 2005). Although RETA proved to be superior in terms of directly measuring and controlling shear stress imposed on the sample in real time, it is limited to soils that possess sufficient internal cohesion to stay intact during the test (Crowley et al. 2012a).

Sediment Erosion Rate Flume

The Sediment Erosion Rate Flume (SERF) is a device designed to omit operator dependency from an erosion test and provide near-instantaneous erosion rates (Crowley et al. 2012b). It is equipped with a computerized sample advancement mechanism, a shear stress sensor, and pressure transducers in order to evaluate the shear stress imposed on the sample. Erosion rate is given as distance of sample advancement per time.

A schematic of SERF is shown in Fig. 17. The device is comprised of two water pumps, a 2.74 m long aluminum rectangular flume with cross-sectional dimensions of 5.08 x 20.32 cm,

wall thickness of 1.27 cm, a temperature probe, a cooling system, a flow straightener, pressure ports, a shear stress sensor, an ultrasonic ranging system, fiber optic lasers, and photoelectric sensors. The flow straightener is located in the first 0.3 m of the flume; after passing through the flow straightener, water passes over the shear stress sensor with two pressure ports attached to each end of the sensor to provide a comparison between measured and computed shear stresses. Another set of pressure ports are located upstream and downstream from the sample. The bottom of the flume contains a circular opening into which a tube containing the sample can be inserted. Above the opening, inside the flume, resides the ultrasonic ranging system to monitor erosion depth. The bottom of the flume has six 1.5 mm grooves to house three fiber-optic lasers and their corresponding photoelectric sensors. Fig. 18 shows the locations of the ultrasonic ranging system, lasers and their corresponding sensors, and a pressure port (Crowley et al. 2012a; Crowley et al. 2012b; Sheppard and Bloomquist 2005).

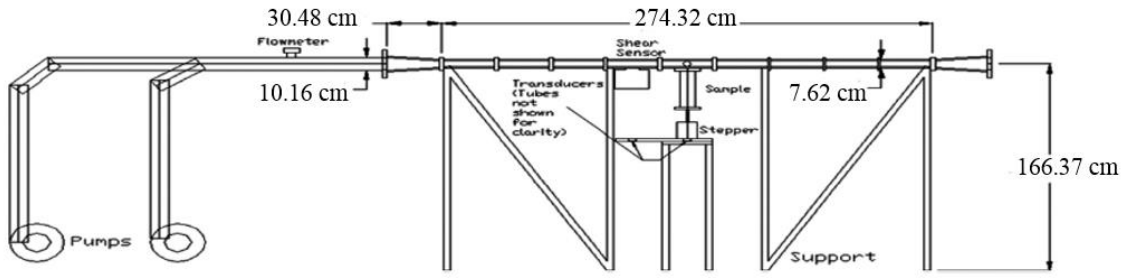

Fig. 17. Schematic of SERF (Adapted from Crowley et al. 2012b)

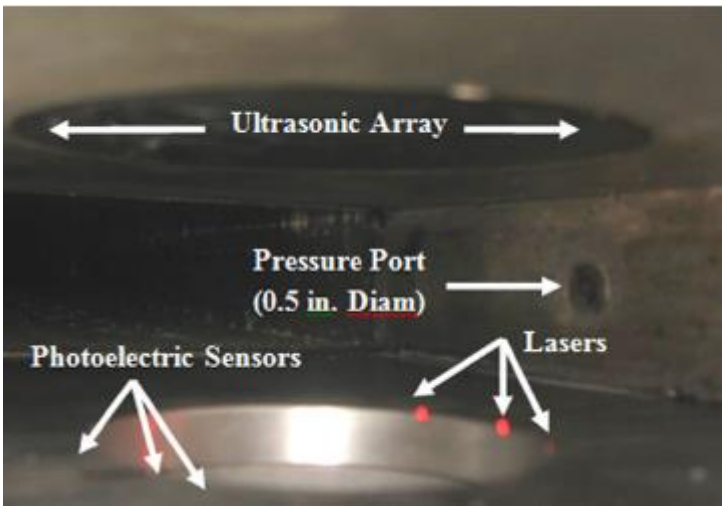

Fig. 18. SERF's ultrasonic and laser system (Crowley et al. 2012b)

The ultrasonic ranging system and fiber-optic lasers can be engaged simultaneously or individually as the erosion depth monitoring system and sample self-advancement. In testing some soil types, such as clay, the ultrasonic rays can penetrate a layer of the sample, thereby giving false readings. Therefore, using fiber-optic lasers exclusively yields greater accuracy (Crowley et al. 2012b).

SERF is advantageous because it can be used on fine-grained or coarse-grained soils with or without internal cohesion, it omits operator dependency, and it provides real-time erosion rate data. SERF is also equipped with a cooling system to maintain a constant water temperature (Crowley et al. 2012b). A drawback of SERF is the inability to maintain average shear stress throughout the test.

Sediment Erosion at Depth Flume

McNeil et al. (1996) and Ravens (2007) described the Sediment Erosion at Depth Flume (SEDFlume) as a straight flume that can be employed to measure rate of erosion of sediment. SEDFlume is comprised of a 120 cm inlet section that straightens the water flow and assures the

flow is fully developed, meaning that the velocity profile is parabolic in shape and remains unchanged in the direction of flow. The inlet section is attached to a 15 cm test section with identical cross-sectional dimensions and an opening at the bottom of the flume into which the coring tube can be inserted, a coring tube, flow exit section, water storage tank, and a water pump. The coring tube is rectangular and has cross-sectional dimensions of 10 x 15 cm and 1 m in length. The inlet section is a rectangular duct with cross-sectional dimensions of 10 x 2 cm. A schematic of SEDFlume is shown in Fig. 19.

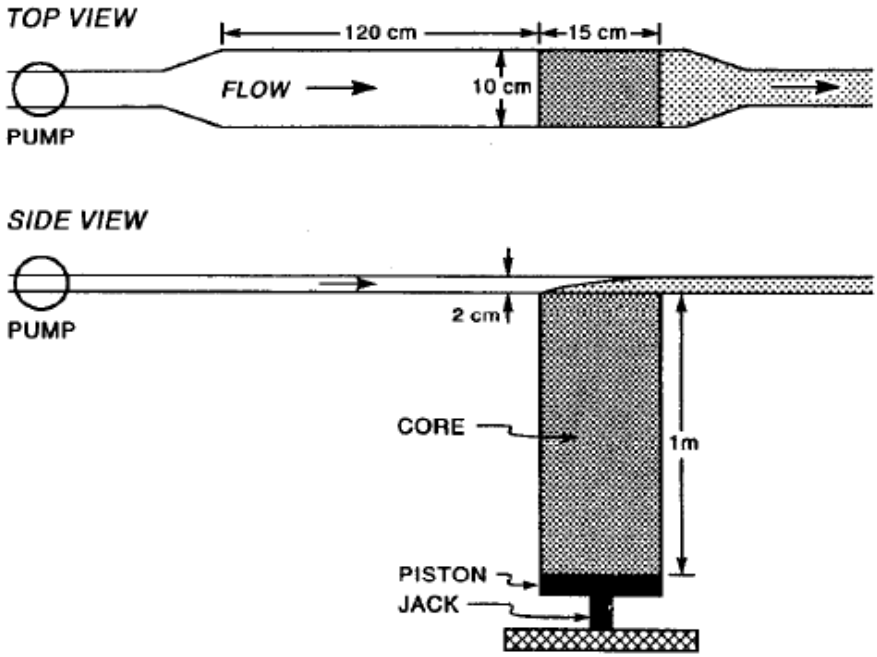

Fig. 19. Schematic of SEDFlume (McNeil et al. 1996)

SEDFlume operates by pumping water through the inlet section where the water passes through flow strengtheners. Flow is allowed to fully develop, achieving its parabolic velocity profile. Next, the flow enters the test section where it passes over the sediment sample; erosion can be observed if the shear stress is imposed is equivalent to or exceeds the critical shear stress.

A piston beneath the core sample is linked to a motor with which an operator is able to advance or recede the sample contained within the coring tube, in order to maintain the samples surface flush with the test conduits bottom. Erosion rate is presented as the distance the piston advances per time (McNeil et al. 1996). Similar to the FLUME, Eq 2, Eq 3, and Eq 4 calculate shear stress, the friction factor assuming a smooth bottom, and the Reynolds number, respectively. SEDFlume can be employed to perform two types of experiments: determination of critical shear stress as a function of depth and determination of erosion rate as a function of shear stress and depth (McNeil et al. 1996).

McNeil et al. (1996) stated that in cases in which undisturbed samples were used, SEDFlume is disadvantageous because the conduit is only 2 cm in height and any large sized debris contained in the sample must be removed in order to proceed with the test. When a large number of large sized debris are present within the sample, SEDFlume cannot be employed. Other disadvantages of the SEDFlume include its operator dependency, its inability to maintain a constant shear stress throughout a test, and its limitations to measure bulk erosion rates without providing information about transport mechanisms of eroded particles (Roberts et al. 2003). Advantages of the SEDFlume include its ability to test fine-grained and coarse-grained soils from the field or remolded in the laboratory, and its allowance of examination of sediment erodibility with depth.

Adjustable Shear Stress Erosion and Transport

Roberts et al. (2003) the Adjustable Shear Stress Erosion and Transport (ASSET) flume is designed to quantify erosion of sediments while concurrently investigating the eroded particle's transport mode. As a successor of the SEDFlume, ASSET retains all the capabilities of its predecessor in addition to revealing the transport mode of eroded particles.

Roberts et al. (2003) described ASSET's test section as identical in design and operation to SEDFlume, with the exception that ASSET has a slightly taller channel. ASSET consists of a water reservoir, a centrifugal pump, a motor-controlled screw jack, an erosion channel and a test section, a transport channel equipped with bedload traps, a flowmeter, and connective plumbing. The channel has cross-sectional dimensions of 5 x 10.5 cm, resulting in a conduit that is 3 cm taller than its predecessor. Flow is allowed to develop in the 180 cm rectangular conduit before entering the test section.

An operator-controlled screw jack pushes sediment through the tube into the flume so that the sediment's surface remains flush with the conduit's bottom at all times. The tube containing the sediment core is rectangular with crosssectional dimensions of 15 x 10 cm and 1 m in length. After passing over the test section, the flow enters the transport channel in which three traps exist downstream. The first trap is located 1 m downstream from the test section, followed by the remaining two traps located at 1 m intervals from the center of the preceding trap. Each trap has dimensions of 15 x 10.5 cm and capture basins that are 10 cm deep occupying a volume of 2 l. In order to eliminate resuspension of trapped sediment, each trap is equipped with a baffle system, further reducing recirculation (Roberts et al. 2003). Erosion rates are presented as distance per time, similar to SEDFlume. A schematic of ASSET showing the flume channel duct, sediment core, erosion test section, and first bedload trap are shown in Fig. 20.

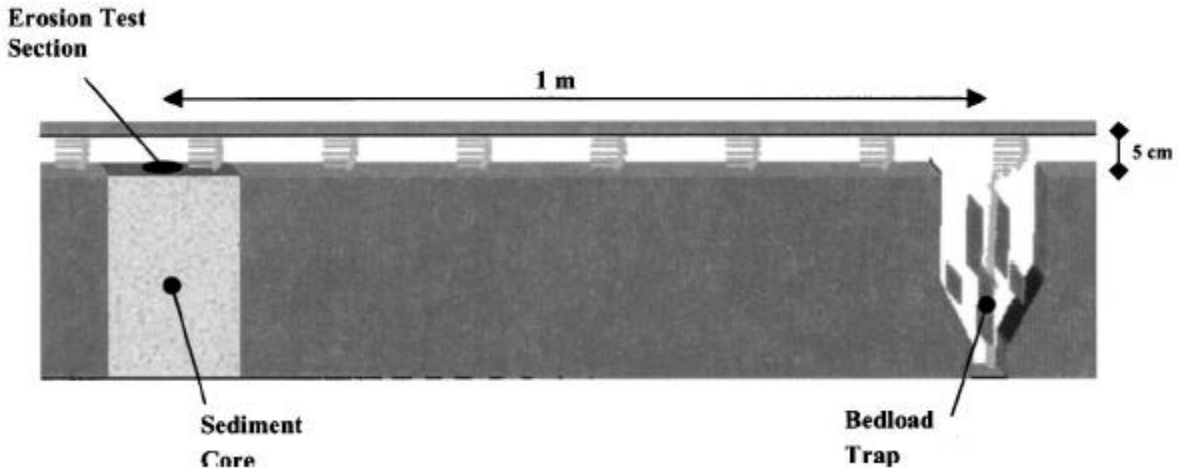

Fig. 20. Schematic of ASSET (Roberts et al. 2003)

Advantages of ASSET include its ability to test fine-grained and coarse-grained soils from the field or remolded in the laboratory and its allowance of inspection of sediment erodibility with depth while revealing the particles transport mechanism. ASSET also can be employed to determine critical shear stress with depth and erosion rate as a function of shear stress and depth. Disadvantages of ASSET are its inability to maintain a constant shear stress throughout the test and its operator dependency.

Recirculating Flume

In the study by Schaaff et al. (2006), the recirculating flume consists of 3.6 m long PVC pipe filled with 300 l of water. Dimensions of the test section were 0.4 x 0.4 m. Four specimens were contained in PVC rings that were 10 cm in height; the test specimens were inserted 2.1 m downstream of the main channel. The motor-induced flow velocity ranges from 0 to 32 cm/s. Two honeycomb structures are placed at the entrance of the main channel to break up large clumps of material entering the flow channel, and a turbidity sensor was located downstream from the test section. Erosion rates were expressed as mass per area per time. A schematic of the recirculating flume is shown in Fig. 21. One advantage of the recirculating flume is that erosion

can be measured with a turbidity sensor by collecting water samples every 3 min. and filtering out suspended particulate matter in order to calibrate the sensor. In addition, the recirculating flume can be utilized on fine-grained and course-grained sediment from the field or reconstituted in the laboratory. Major drawbacks of the recirculating flume are the inability to control shear stress imposed on the soil sample, requirement of continuous recalibration of the sensor due to recirculation of sediment, and the possibility of achieving only low flow velocities.

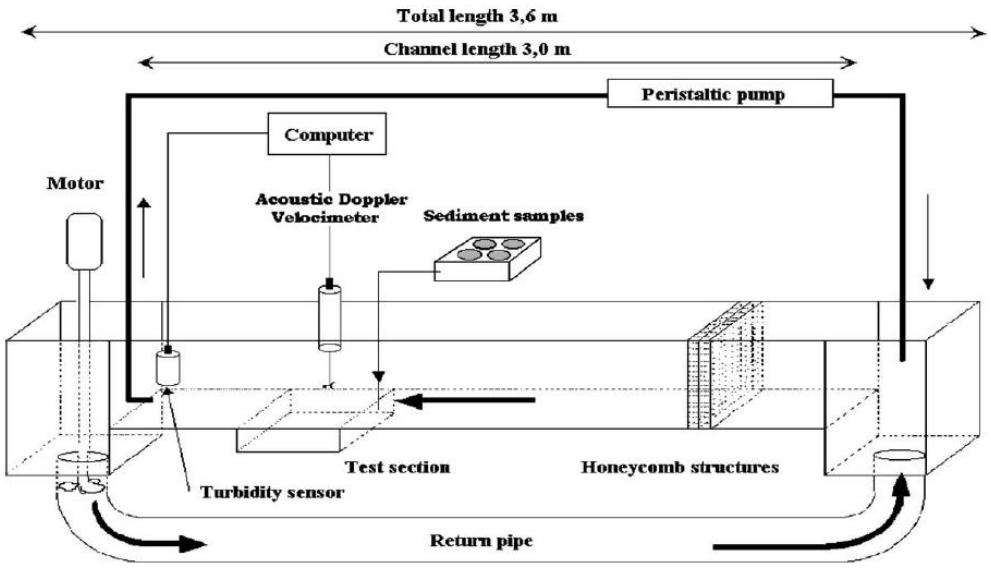

Fig. 21. Recirculating flume (Schaaff et al. 2006)

Turbidity

Davies-Colley and Smith (2001) referred to nephelometric turbidity as an index of light scattering by suspended particles measured in Nephelometric Turbidity Units (NTUs). Turbidity is a phenomenon that describes the cloudy appearance in water. Nephelometric turbidity is a relative index of light scattering; it is not to be considered a scientific measurement until it is cross-calibrated to concentration of suspended solids (Davies-Colley and Smith 2001).

Attenuation of light in a liquid media by suspended particles is greatly influenced by the concentration of suspended particles, particle size, and particle size distribution. Because turbidity sensors are calibrated with a standard scattering material, formazin or SDVB, no direct correlation exists between NTU and Suspended Solid Concentration (SSC) for all particle sizes. Moreover, each soil type may have a unique correlation between NTU measurements and SSC. Fig. 22 shows a plot of variation in particle size distribution of turbidity standards, formazin and SDVB, and suspended sediment in rivers and oceans. In correlating NTU to SSC a problem is encountered when light attenuation from the suspended solids does not match light attenuation of the standard formazin or SDVB, a result of wide range of particle size distribution in the sample leading to weak correlations (Downing 2008).

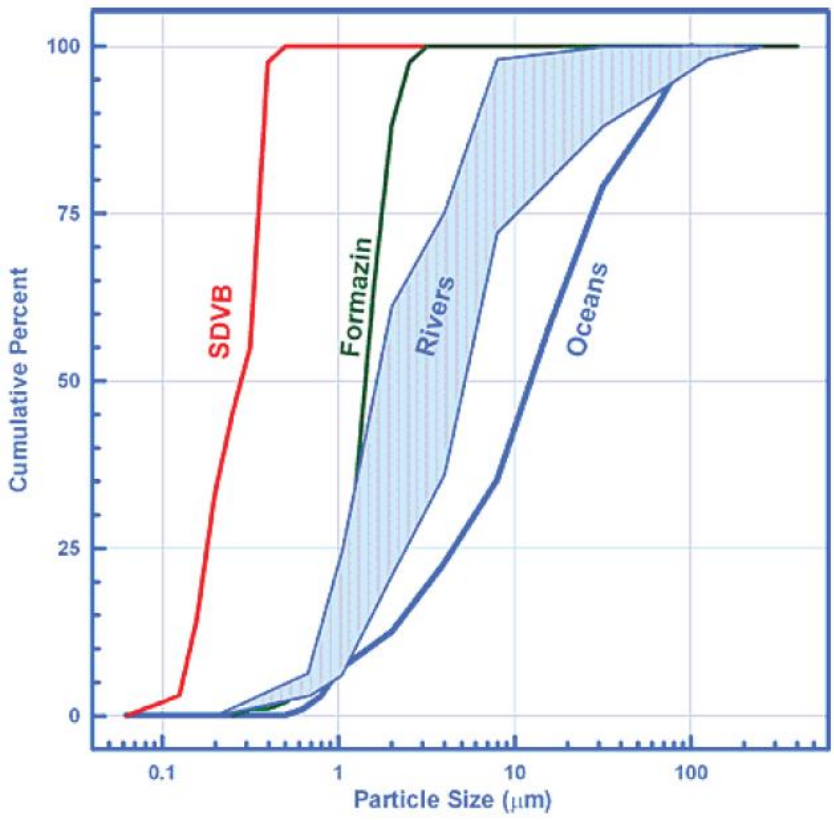

Fig. 22. Variation of particle size distribution of turbidity standards and suspended solids (Downing 2008)

Turbidity Sensor

The recirculating flume (Schaaff et al. 2006), and the FLUME (Ravens 2007; Debnath et al. 2007) utilized turbidity sensors in their erosion measuring devices. Every study the turbidity sensor was used required gathering water samples to further calibrate the sensor and quantify particles in suspension.

Schaaff et al. (2006) utilized a turbidity sensor to measure particles in suspension downstream from the test section of the recirculating flume. Two water samples were collected every 3 min. and were then filtered to quantify the suspended particulate and organic matter in order to further calibrate the turbidity sensor, making the relationship between turbidity measurements and suspended particulate matter possible. Such correlation between turbidity measurements and suspended particulate matter should be performed on each tested soil type because the correlation is unique based on color, particle size, particle size distribution, and shape of particles.

Ravens (2007) used a turbidimeter during the flume in situ testing to obtain particle concentration. In order to relate particle concentration to turbidity measurements, Ravens utilized a calibration curve. This curve, obtained during experiments, was based on the total suspended solids measurements of water samples. Such calibrations showed great agreement with $R^2 \geq 0.85$; however, this calibration curve is unique to each tested soil type.

Debnath et al. (2007) used two turbidity sensors on the flume in situ testing device: One sensor was located at the entrance of the test section to observe background conditions, and the other sensor was mounted downstream from the test section. Turbidity readings were independently calibrated against suspended sediment concentration for each experiment by gathering at least six water samples obtained from sampling locations near the turbidity sensors.

Chapter 3 - Methodology

This chapter describes the preparation of samples tested in this study, the testing procedure in the KSU-EFA and methodology to reduce testing duration. The custom heating system developed to heat samples is discussed, followed by a brief discussion of the turbidity sensor instrumented in this study.

Sample Preparation

A hydrometer test was conducted in compliance with ASTM designation D422-63 in order to analyze particle size and distribution. In this test, 50 g of kaolin clay was mixed with 125 ml of dispersive agent. Hydrometer readings and temperature readings were taken at set time intervals over a period of 25 days. All readings were taken with a 152H hydrometer. Sieve analysis was not performed since the soil in question was clay and all particles were finer than the No. 200 sieve. Results of the hydrometer test are discussed in Chapter 4. A slight deviation from the ASTM standard occurred when the test duration was extended from 1,440 to 36,165 minutes to account for at least 90% of particles which remained in suspension after 1440 minutes.

Manufactured kaolin clay was used to prepare all samples. In order to make identical samples, optimum water content and maximum dry unit weight had to be determined using the Standard Proctor test in compliance with ASTM designation D698-12. Oven-dry soil was mixed with the desired water content and then allowed to rest in a humidity room for 24 hours, allowing the moisture to distribute itself evenly throughout the soil mass. Soil samples were mixed at moisture contents of 26%, 28%, 30%, 32%, and 34%. Following the 24-hour resting period, soil samples were compacted into a 10.16 cm diameter mold in three equal layers using a 24 N

rammer dropped 25 times onto each layer from a distance of 30.5 cm. Samples were then trimmed flush with the mold, and sample weight was recorded. Using the volume of the mold, density was computed by dividing the weight of compacted soil by the volume of mold. The Standard Proctor test was conducted twice. Compaction curves and the average dry unit weight at optimum water content are discussed in Chapter 4.

Samples were prepared by compacting the soil in various numbers of layers and number of hammer drops to replicate the maximum dry unit weight determined by the Standard Proctor test at optimum water content. Two 30.5 cm long Shelby tubes were clamped together where the soil was compacted in order for the sample to occupy the entire length of the tube. Using the same 24 N hammer used in the Standard Proctor test, results showed that compacting a soil sample in three layers with 55 hammer drops per layer to compact clay in a 30.5 cm Shelby tube was sufficient to recreate the maximum dry unit weight determined by the Standard Proctor test. However, when tested in the EFA, results showed no consistency. One sample was tested twice with two velocities, 0.5 and 1 m/s, but results showed large discrepancy in erosion rates within that sample. Results of the two tests performed on the same sample are summarized in Table 3. The maximum difference in erosion rate, when tested at 1 m/s, was 28 mm/hour. This discrepancy was a result of layering since layers experienced various numbers of hammer drops.

Table 3 Results of an EFA test on one sample

Test	Erosion Rate at 0.5 m/s (mm/hour)	Erosion Rate at 1 m/s (mm/hour)
Trial 1	17	36
Trial 2	0	8

An alternate approach was investigated to eliminate the source of error, where the entire soil sample was compacted in one layer while the number of hammer drops was systematically

changed until desired results were achieved. Because the hammer dropped on a circular metal plate, the compaction energy was evenly distributed, allowing the number of hammer drops to reduce to 250–300 drops. Sample results from EFA testing showed similarity in erosion rates and were repeatable across all samples compacted in one layer, Table 1 in Chapter 1 summarizes results of samples tested for consistency. A turbidity sensor was also utilized to confirm similarity between samples. A turbidity plot showing similarity in erosion is presented later on in this chapter for samples tested at 4 m/s. Fig. 23 shows items used in preparing samples, including a hammer, two Shelby tubes, a clamp, and a metal plate.

Fig. 23 Items utilized in sample preparation

Sample Testing

In order to test samples in the EFA, a Shelby tube containing a soil sample was mounted in the test section and clamped onto the adjustable platform. The sample was extruded by advancing the motorized piston, and then the sample was trimmed flush with the Shelby tube's

rim. The adjustable platform was raised into the flume's test section so that the sample's surface was flush with the flume's bottom. Fig. 24 provides a schematic showing the sample mounted in the test section. After the sample was installed, the test was initiated by adjusting the water flow to the desired velocity and allowing the sample to erode over the desired duration. In a standard EFA test, up to six velocities are tested over a period of 1 hour per velocity. However, this study investigated testing at shorter durations of 10 and 30 minutes per velocity. An operator visually monitor the sample through a Plexiglas window in the test section and advance the motorized piston as needed so that the sample's surface remain flush with the flume's bottom at all times. Upon completion of each velocity, the sample was receded from the flume's test section, protruded from the Shelby tube, trimmed flush with the tube's rim before the test was initiated at the subsequent velocity.

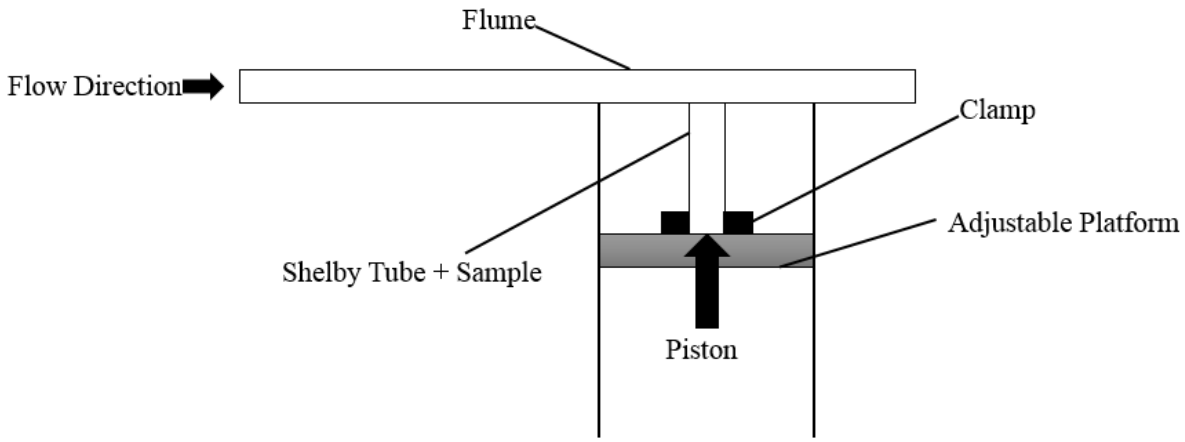

Fig. 24 Schematic of sample mounted in test section

Multiple approaches were investigated in an effort to reduce testing duration. One approach involved conducting a continuous test over a period of 10 minutes per velocity, in which each velocity was sequentially tested without stopping to trim the sample flush before initiating the subsequent velocity. Another approach utilized a discontinuous test at 10 minutes

per velocity, in which the sample was trimmed flush before initiating the subsequent velocity. An approach that used an intermediate duration of 30 minutes per velocity was also investigated. The intermediate duration test was discontinuous; the sample was extruded and trimmed flush following each velocity. Results of the 10-minute tests showed significant underestimation in erodibility. However, results of the 30-minute test showed an agreement with results of a standard test, with a maximum discrepancy of 2 mm/hour at a velocity of 3 m/s. Erodibility plots comparing results of a standard test to results of the shorter-duration tests are shown in Fig. 25.

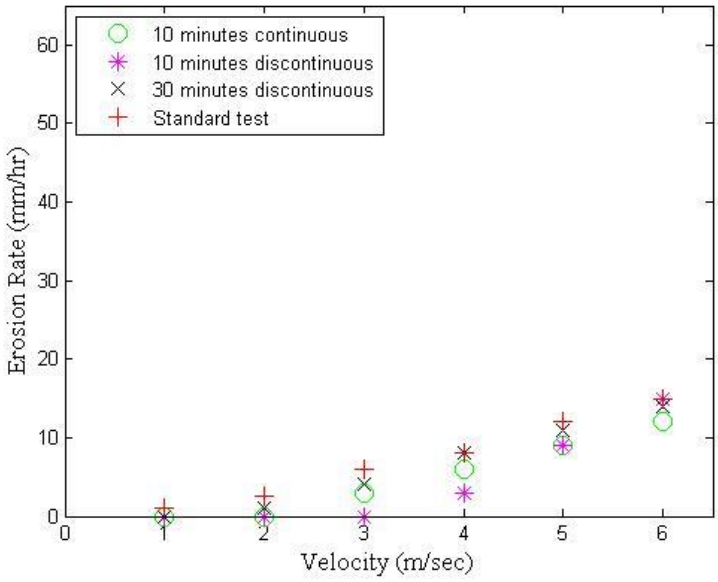

Fig. 25 Erodibility plot comparing results of a standard test to shorter-duration tests

Sample Heating

In this study, a custom heating system was developed to investigate the effects of soil temperature on erosion rate. The heating system was comprised of a heating jacket, a piston head equipped with two thermocouples, a control box, and a National Instrument data acquisition system, NI 9211. A heating jacket, which supplied heat, was wrapped around a 15.24 cm Shelby tube. A piston head equipped with two thermocouples was used to monitor internal soil

temperature. A control box was used to regulate the temperature supplied to the heating jacket, with a maximum setting of 40 ˚C. A data acquisition system and Labview 2014 were used to record and monitor internal temperatures. A schematic of the heating system is presented in Chapter 1. Due to size limitations of the heating jacket and thermocouples, the sample had to be transferred from a 30.5 cm long Shelby tube to a 15.24 cm long Shelby tube using the EFA's sample advancement mechanism. By clamping both tubes together and extruding 15.24 cm, the sample transfer was complete. A minimum of 30–45 minutes was allowed for the sample to heat up from room temperature to desired temperature.

Turbidity Sensor

A Confab Instrumentation inflow turbidimeter, model 850i, was instrumented in this study. The turbidimeter consisted of a sensor and a control box that displayed real-time data. A National Instrument data acquisition system, NI 9203, was also used to log and monitor sensor readings. Labview 2014, the software provided with the data logger, was programmed to record turbidity measurements and time elapsed. Initially, the sensors sampling rate was set to a rate of 100 readings per second. However, due to the large number of data points recorded for every test, the determination was made that reducing the sampling rate to 1 reading per second was sufficient without jeopardizing the resolution. Additional information about the turbidity sensor and its operation is provided in Chapters 1 and 2. An example of sensor results presented in Fig. 26, confirming similarity in erosion of two samples tested under a flow velocity of 4 m/s.

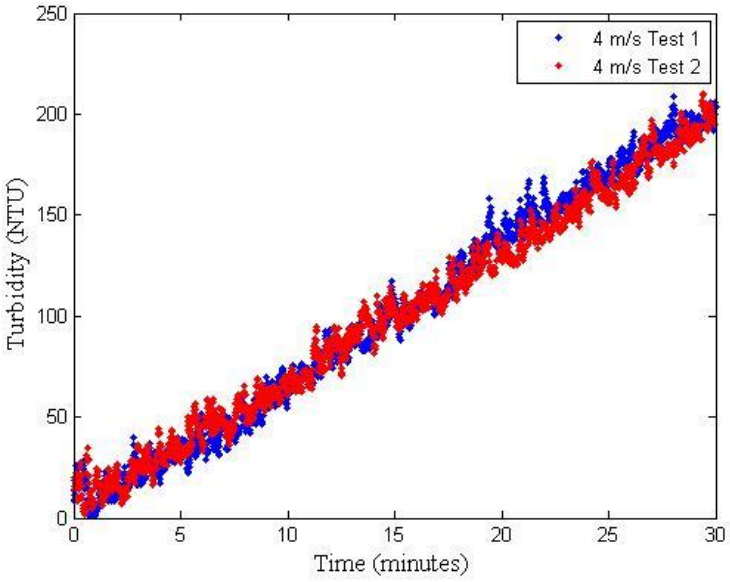

Fig. 26 Turbidity plot confirming similarity in erosion

PVC pipes guided the water flow from the flume back into the water reservoir. The sensor was located, in the PVC pipe, downstream from the sample's test section in order to measure water turbidity as erosion occurred and to avoid interrupting the flow regime. Multiple sensor locations were investigated. Initially the sensor was installed in the top section of the PVC pipe, as shown in Fig. 27, but the sensor was not fully submerged into the flow at low velocities. Therefore, the sensor was relocated to another section in the PVC pipe where it was fully submerged regardless of velocity.

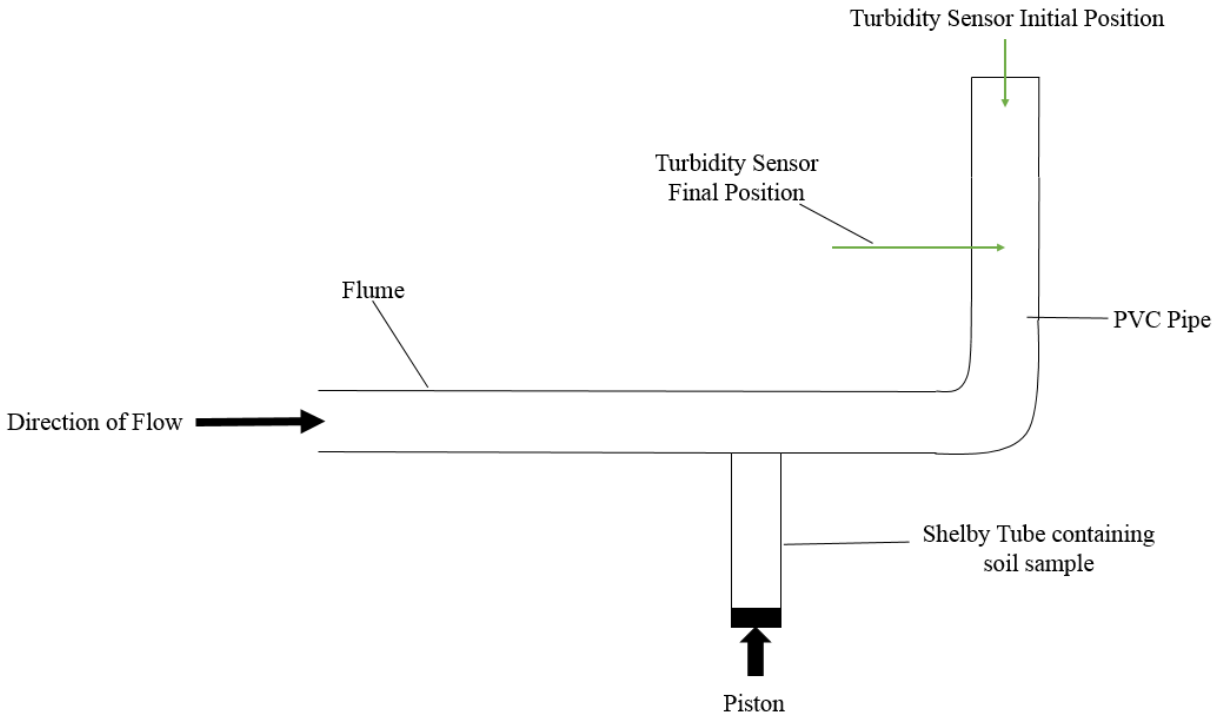

Fig. 27 Schematic of EFA's test section with sensor locations

The effects of increasing water temperature on turbidity measurements were investigated. The sensor was employed as clean water circulated through the system, demonstrating an inverse relationship between turbidity measurements and water temperature. When circulating clean water, the only source that caused turbidity was air bubbles. As the temperature of the circulating water increased, turbidity measurements decreased, potentially showing that warm water is less capable of retaining air bubbles than cold water. However, additional testing to quantify air bubbles is required but is beyond the realm of this study. Turbidity measurements obtained from the sensor was plotted against temperature, as shown in Fig. 28. The initial water temperature was approximately 17 ˚C; that temperature was allowed to increase to approximately 30 ˚C over a period of 30 minutes.

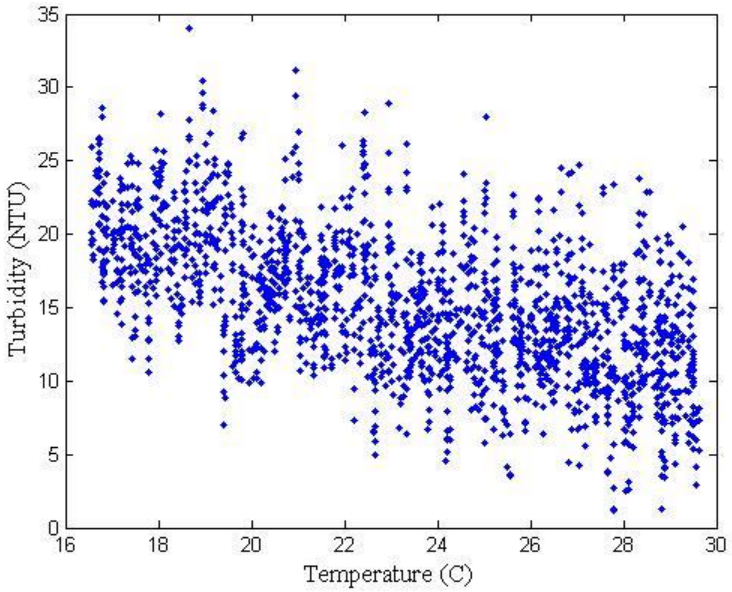

Fig. 28: Turbidity measurements against temperature as clean water circulated

In summary, the first step of making consistent samples in this study was to conduct a Standard Proctor test on kaolin clay to determine optimum water content and maximum dry unit weight. Soil samples were compacted in Shelby tubes in one layer in order to eliminate the effects of layering. A turbidity sensor was instrumented and used to confirm similarity in erosion across samples. The main goal of implementing a turbidity sensor was to measure water turbidity as erosion occurred. A custom heating system was developed to study the effects of increased soil temperature on erosion rate. This study also reduced test duration from 1 hour to 30 minutes per velocity without jeopardizing the results.

Chapter 4 - Results and Discussion

This section includes results of the hydrometer and Standard Proctor tests conducted on kaolin clay and results of a standard EFA test conducted on room temperature samples when the temperature of the circulating water was allowed to increase. Results of heated and room temperature samples are presented and discussed, showing the effects of increased temperatures on erosion rates of fine-grained soils. In addition, results of room temperature samples are included in which the temperature of the circulating water was controlled. Finally, results obtained from the turbidity sensor instrumented in this study are discussed.

Particle Size Analysis

In accordance with ASTM designation D422-63, a hydrometer test was conducted to measure particle size and particle size distribution. The test was initiated by mixing 50 g of manufactured kaolin clay with 125 ml of dispersing agent and adding distilled water to a total volume of 1000 ml. Hydrometer readings and temperature were measured at set time intervals over a period of 25 days. Particle diameter was calculated by

$$D = K\sqrt{L/T}, \qquad \textbf{Eq 6}$$

where D is particle diameter, K is constant depending on temperature and specific gravity, L is effective depth, and T is time interval. In order to compute the fraction of sediment still in suspension (i.e., percent finer), the following mathematical expression was utilized:

$$P = \left(\frac{Ra}{W}\right)*100, \qquad \textbf{Eq 7}$$

where P is the percentage of soil remaining in suspension, R is the corrected hydrometer reading, a is a correction factor based on specific gravity, and W is oven dry mass of soil.

Using the computation of particle size and the percentage of particles remaining in suspension, particle size distribution was plotted, as shown in Fig. 29. The ASTM standard requires that the test be carried out over a period of 24 hours; however, a slight deviation from the standard occurred when the test was allowed to commence over a period of approximately 603 hours since more than half of the particles remained in suspension after 24 hours.

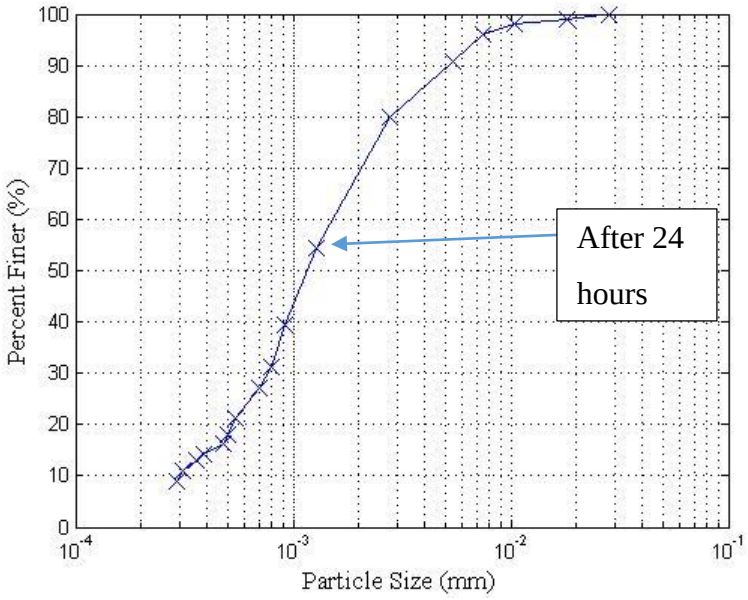

Fig. 29 Particle size distribution of kaolin clay

Findings of hydrometer test conducted indicated that more than 90% of particle sizes measured between 0.028 and 0.00029 mm; 99.99% of the particles were finer than 0.028 mm and 9.09% were finer than 0.00029 mm.

Standard Proctor Test

In this study the Standard Proctor test was performed twice on the kaolin clay in order to confirm results. Soil samples were mixed and compacted at moisture contents of 26%, 28%, 30%, 32%, and 34%. Computed dry unit weights of both Standard Proctor tests are presented in Table 4 and the corresponding compaction curves are shown in Fig. 30.

Table 4 Results of the Standard Proctor tests

Moisture Content (%)	Dry Unit Weight (kN/m^3) First Test	Dry Unit Weight (kN/m^3) Second Test
26	12.94	13.19
28	14.18	14.06
30	14.14	14.06
32	13.55	13.61
34	13.05	13.08

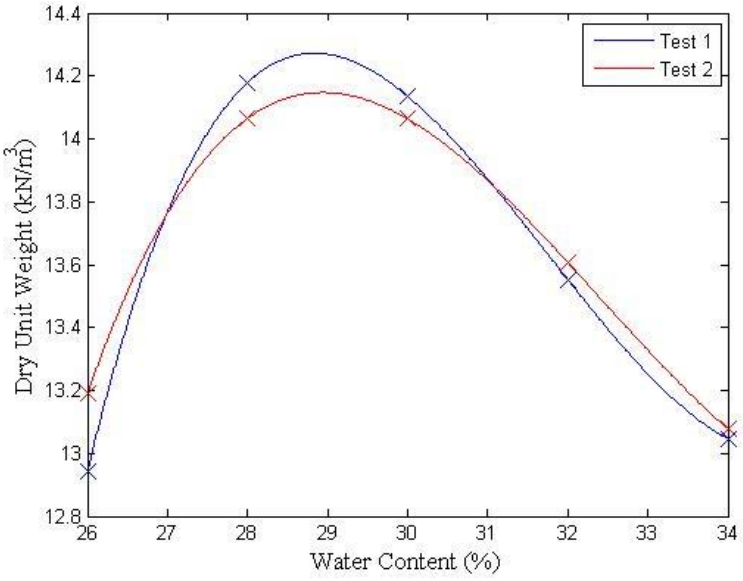

Fig. 30 Compaction curves of manufactured kaolin clay

Dry unit weights were computed using the following mathematical expressions:

$$\gamma_d = \frac{\gamma_m}{1+w}, \quad \textbf{Eq 8}$$

where γ_d is dry unit weight and *w* is water content. The moist unit weight, γ_m is

$$\gamma_m = \frac{M_s}{V} * 0.0098, \quad \textbf{Eq 9}$$

where M_s is mass of compacted soil, V is volume of mold, and 0.0098 km/s^2 is acceleration due to gravity. The compaction curve showed that maximum dry unit weight was achieved at a moisture content of 29% in both tests. Maximum dry unit weights were 14.27 and 14.18 kN/m^3 for the first and second tests, respectively, with an average value of 14.23 kN/m^3. Based on results, samples compacted to dry unit weights of 14.23 kN/m^3 ± 1 kN/m^3 at 29% water content were deemed acceptable for the purposes of this study. Table 1 confirms similar erodibility across samples prepared and tested in the same manner.

Effects of Soil Temperature

A standard EFA test encompassed testing up to six velocities over a duration of 1 hour per velocity. The sample was extruded after each velocity and trimmed flush before initiating the subsequent velocity. Results of the standard test were used as baseline for comparison of tests conducted on heated samples. An erodibility plot summarizing results of the standard test is presented in Fig. 31. As water circulated through the system, its temperature increased due to energy conversion. In this test, the water's temperature was allowed to increase. Test results of when the temperature of the circulating water was controlled are presented and discussed later in this chapter. The effects of controlled water temperature tests were insignificant on the measured erodibility so the circulating water was allowed to increase in order to utilize the turbidity sensor.

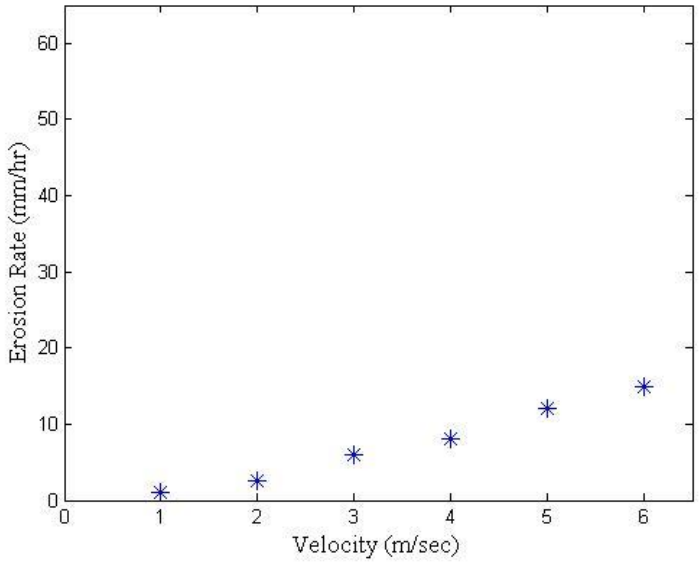

Fig. 31 Erodibility plot of a standard test

In order to test soil temperature effects on erosion rate, a sample was heated to an average temperature of 32 ˚C and tested in accordance with the standard test. Samples were heated using the custom heating system described in Chapter 3. Fig. 32 shows an erodibility plot of a standard test conducted on a sample heated to 32 ˚C. Comparing Fig. 31 and Fig. 32, results indicated a direct relationship between soil temperature and erodibility: Heated samples resulted in more erosion than room temperature samples.

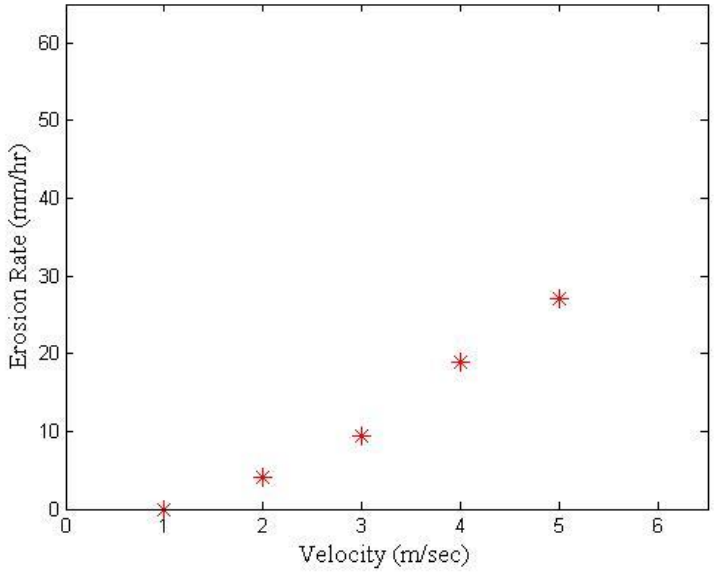

Fig. 32 Erodibility plot of a standard test conducted on a heated sample

Fig. 33 combines Fig. 31 and Fig. 32 in order to directly compare results of a standard test conducted on a room temperature sample (21 ˚C) to results of a standard test conducted on a heated sample (32 ˚C). Results showed that, not only did the heated sample result in a higher erosion rate, the gap between erosion rates grew wider with increased velocities. However, the heated sample was not tested under a velocity of 6 m/s because the water flow pump overheated. A sample at room temperature was tested under a velocity of 6 m/s; results showed that erosion rate at 6 m/s was significantly less than the heated sample's erosion rate when tested under 4 m/s, as shown in Fig. 33. Table 5 shows temperatures, measured dry unit weights, measured water contents, and erosion rates of tests conducted on room temperature and heated samples.

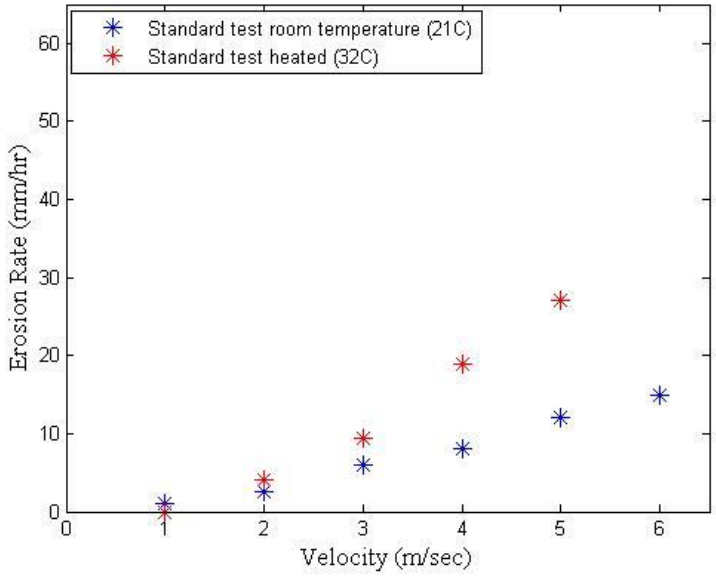

Fig. 33 Erodibility plot comparing heated to room temperature samples

Six samples were heated to temperatures between 30 and 37 ˚C and tested under various velocities. In addition, eight samples were tested at a room temperature of 21 ˚C. However, not all samples were tested under all six velocities. Results of 14 samples are summarized and presented in Table 5 and Fig. 34. In Table 5, samples labeled with the letter H denote heated samples, whereas samples labeled with R stand for room temperature samples at 21 ˚C.

Table 5 Results of room temperature and heated samples

Sample	Temperature (˚C)	Dry Unit Weight (kN/m^3)	Water Content (%)	1 m/s (mm/hr)	2 m/s (mm/hr)	3 m/s (mm/hr)	4 m/s (mm/hr)	5 m/s (mm/hr)	6 m/s (mm/hr)
H-1	30	14.63	29.19	0	3	9	17	NA	NA
H-2	32	14.64	29.33	0	4	9.5	19	27	NA
H-3	34	14.69	29.10	0	3	9	15	24	NA
H-4	34	14.76	29.00	0	3	12	21	NA	NA
H-5	35	14.63	29.19	0	3	9	18	42	NA
H-6	37	14.64	29.33	0	3	9	15	24	60
R-1	21	14.62	29.04	NA	NA	NA	6	9	12
R-2	21	14.62	29.04	1	2.5	6	8	12	15
R-3	21	14.80	28.00	0	0	9	12	NA	NA
R-4	21	14.70	29.30	0	1	5	10	NA	NA
R-5	21	14.70	29.30	0	0	4	9	11	13
R-6	21	14.70	29.30	0	1	4	8	11	14
R-7	21	14.66	29.00	NA	0	NA	6	12	NA
R-8	21	14.31	NA	NA	NA	NA	6	12	NA

Fig. 34 shows that the heated samples had greater erosion rates than the room temperature samples. There is a need to test between 21 and 30 °C to identify how small of a temperature change affects soil erodibility.

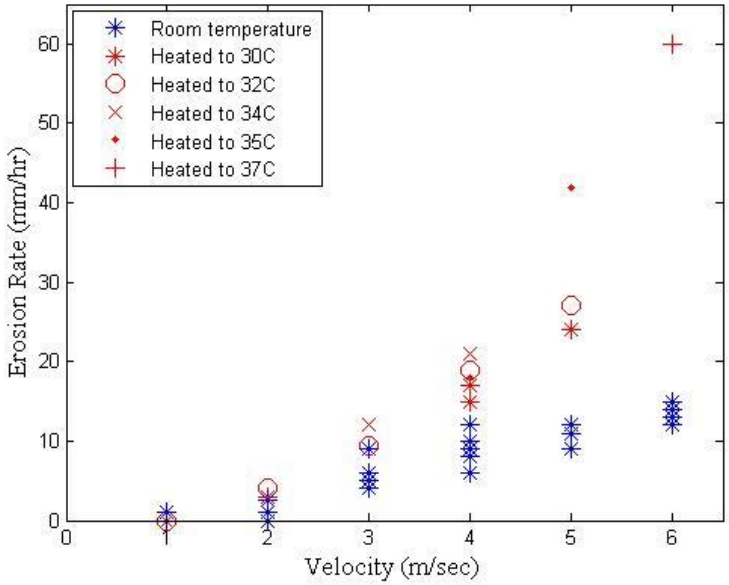

Fig. 34 Erosion rate comparing room temperature samples to heated samples

Effects of Water Temperature

As water circulates through the EFA, it warms due to energy conversion from kinetic to thermal energy. A standard test was conducted that allowed the circulating fluid's temperature to rise from 16 to 30 ˚C for each velocity. Fig. 35 shows results of the standard test as water temperature rose for velocities of 1–6 m/s.

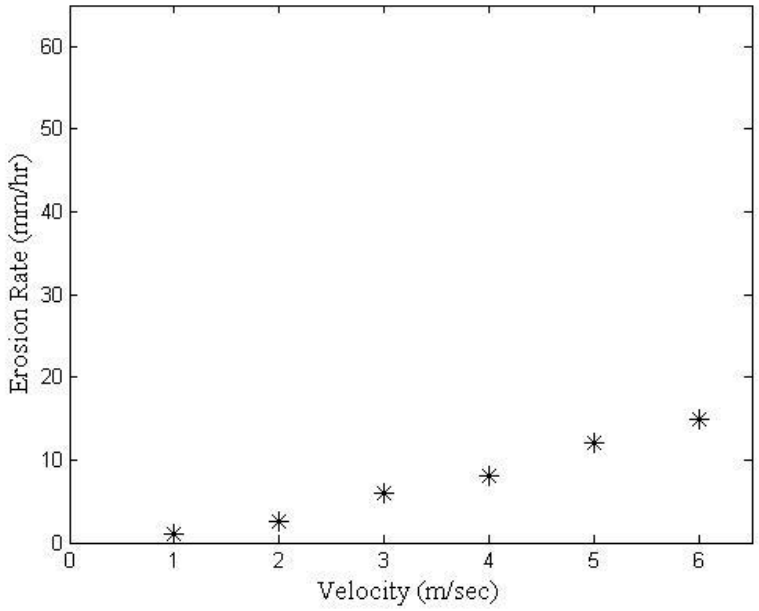

Fig. 35 Erodibility plot of a standard test allowing water temperature to increase from 16 to 30 ˚C

In order to confirm the effects of increasing water temperature on soil erodibility, another standard test was conducted twice while maintaining water temperature between 16 and 20 ˚C. The control on water temperature was achieved by simultaneously draining and filling the system. Results of the controlled water temperature tests are summarized in Fig. 36; velocities tested were 1–5 m/s.

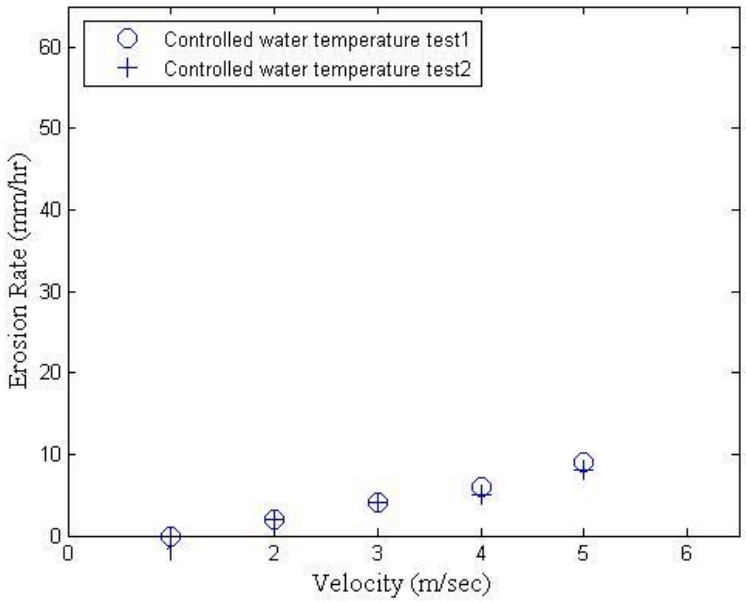

Fig. 36 Erodibility plot of standard tests maintaining water temperature between 16 and 20 ˚C

Samples tested while allowing the circulating water's temperature to rise demonstrated increased erosion compared to samples tested under controlled water temperature, as also shown in the findings of Larionov et al. (2014). In this study the test was initiated at water temperature of 16 °C and was allowed to gradually increase to 30 °C. Whereas Larionov et al. (2014) conducted the tests at constant water temperatures ranging from 0 to 25 °C. Fig. 37 shows an erodibility plot that compares results of standard tests with controlled water temperature to a standard test with warming water. As shown in the figure, samples demonstrated increased erosion for every velocity. The difference in erosion rate ranged from 0.5 mm/hour at 2 m/s to 3 mm/hour at 5 m/s.

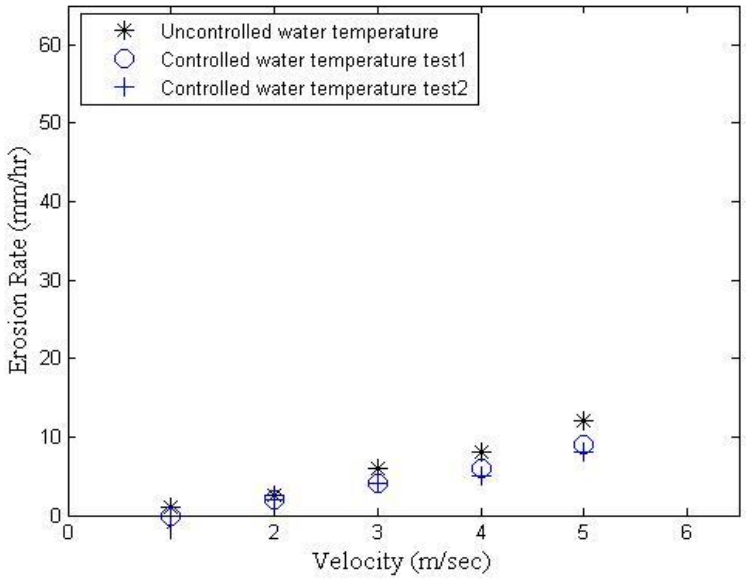

Fig. 37 Erodibility plot comparing results under controlled and uncontrolled water temperatures

The difference in erosion rate of samples tested under controlled and uncontrolled water temperatures was not significant because all tests were initiated at water temperature of approximately 16 ˚C and it progressively got warmer. For controlled water temperature tests, though, water temperatures were maintained between 16 and 20 ˚C. In order to study the comprehensive effects of water temperature on erosion rates, tests should be initiated and maintained at various water temperatures, as done by Larionov et al. (2014). Results of water temperature effects are summarized in Table 6. Based on the small difference in erosion rates between uncontrolled and controlled water temperature, water temperatures were not controlled in the majority of these tests because the difference was insignificant.

Table 6 Results of tests conducted under controlled and uncontrolled water temperatures

Test ID	Dry Unit Weight (kN/m3)	Water Content (%)	1 m/s (mm/hr)	2 m/s (mm/hr)	3 m/s (mm/hr)	4 m/s (mm/hr)	5 m/s (mm/hr)
Uncontrolled Water Temperature	14.62	29.04	1	2.5	6	8	12
Controlled Water Temperature Test 1	14.60	29.80	0	2	4	6	9
Controlled Water Temperature Test 2	14.56	28.50	0	2	4	5	8

Turbidity Sensor

Inflow turbidimeter model 850i was implemented in this study to map soil erosion. As soil erodes, water clarity is affected as a result of continuous mixing; therefore, data collected from the sensor were used to confirm visual observation of soil erosion. Fig. 38 shows turbidity measurements of a test conducted twice over a period of 30 minutes. The only difference was that one sample eroded 0.5 mm more than the other. The sole purpose of this figure was to demonstrate sensor sensitivity in measuring minute differences in erosion. In every turbidity plot presented in this study, turbidity measurements were normalized by equating the minimum value to zero, allowing effects of air bubbles and any soil remaining in the system from previous tests to be neglected.

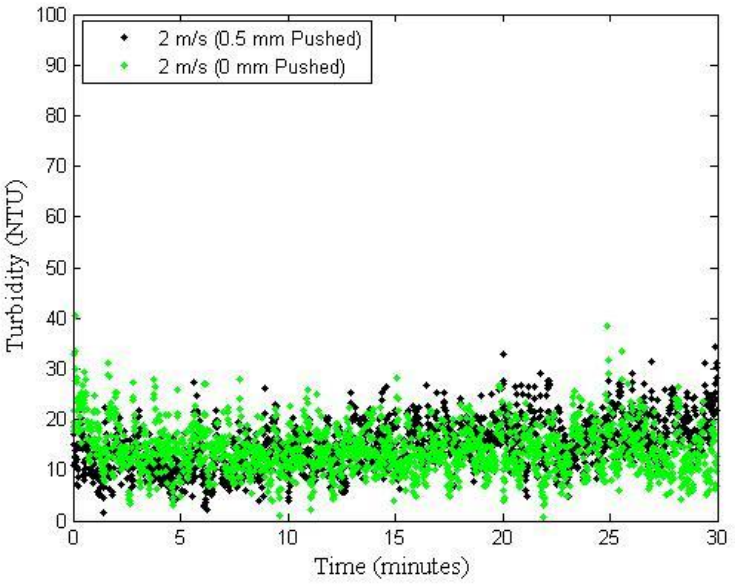

Fig. 38 Turbidity plot demonstrating sensor sensitivity

As demonstrated in Chapter 3 and discussed in this chapter, turbidity measurements of clean water decreased as temperature increased. Therefore, turbidity measurements that remained constant throughout a test in which temperature increased indicated the occurrence of erosion. As shown in Fig. 38, turbidity measurements represented by green dots were constant throughout the test, indicating that erosion took place, although not enough to extrude the sample into the flume.

Another test was conducted twice on the same soil sample over a period of 1 hour in which equal amounts of erosion occurred. As shown in Fig. 39, turbidity plots of tests 1 and 2 overlapped one another throughout the test, indicating equal amounts of soil mixed and further proving the need for this kind of sensor to confirm visual observations of the operator and compare erosion of samples tested at identical velocities.

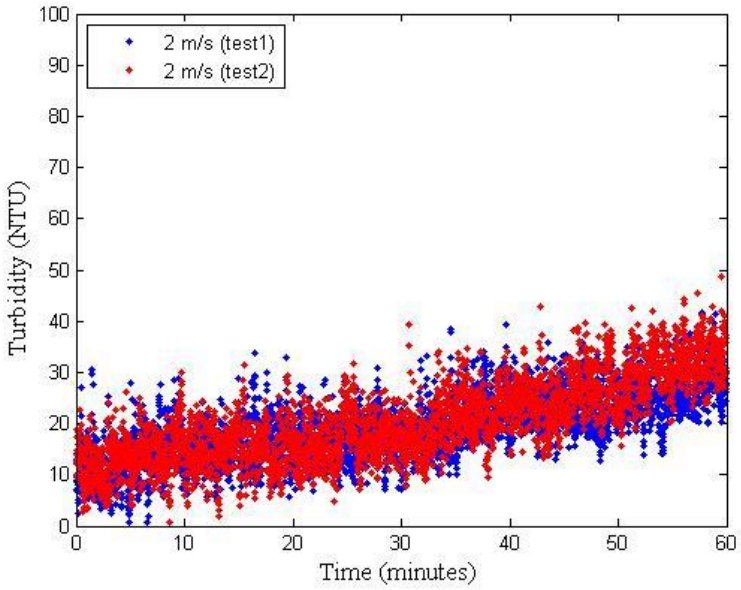

Fig. 39 Turbidity plots confirming equal amounts of erosion

The sensor was tested with only clean water circulating through the system, and the water's temperature was allowed to increase from 16 ˚C to 29 ˚C over a period of 30 minutes. Results showed that turbidity measurements decreased as water temperature increased, as shown in Chapter 3 Fig. 28. Because air bubbles were the only source that caused the water to be turbid and because warm water is less turbid than cold water, the hypothesis in this study was that warm water is less capable of retaining air bubbles than cold water.

The sensor was also employed on a standard test in which erosion was mapped for each velocity and turbidity measurements were combined together in one plot, as shown in Fig. 40. Each color signifies a unique velocity. Velocities 2, 3, 4, and 5 m/s are shown; turbidity measurements of 1 and 6 m/s had to be excluded for visual clarity and to avoid overlapping because the wide range of values would have covered the entire plot.

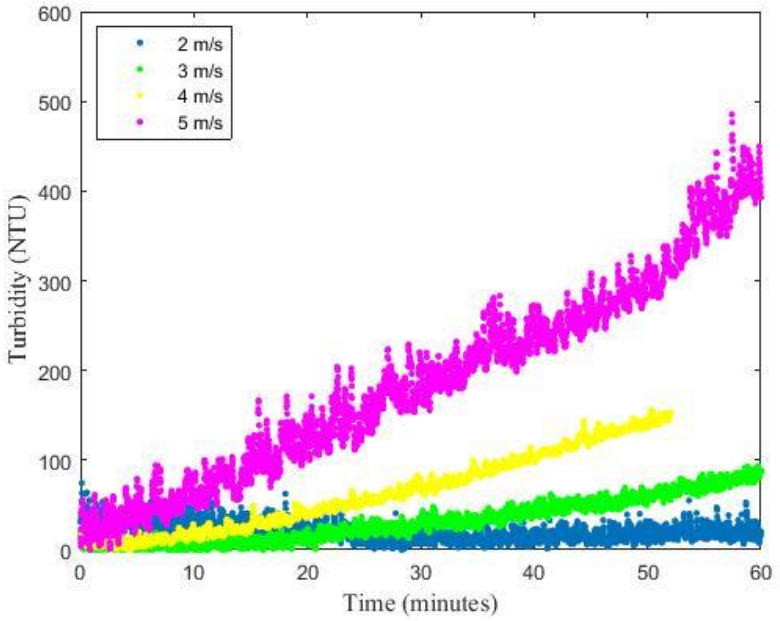

Fig. 40 Turbidity plot of a standard test on room temperature sample, all velocities combined

Similarly, a turbidity plot of a standard test conducted on a heated sample is shown in Fig. 41. Velocities 2, 3, 4, and 5 m/s are shown for the same reasons stated above.

Turbidity Sensor on Heated Sample

The sensor was employed to compare erodibility of standard tests conducted on room temperature and heated samples. Turbidity measurements for velocities 3, 4, and 5 m/s of room temperature and heated samples were plotted in Fig. 42. The turbidity plot represents tests summarized in Fig. 33.

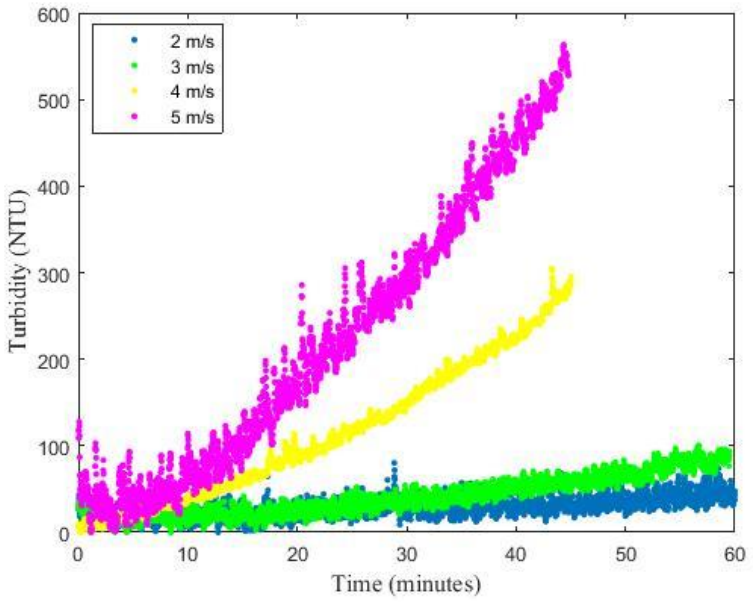

Fig. 41 Turbidity plot of a standard test on heated sample, all velocities combined

Turbidity measurements of the heated sample tested at 4 m/s were equivalent to turbidity measurements of the room temperature sample tested at 5 m/s; however, the turbidity measurement slope of the heated sample at 4 m/s was steeper than the turbidity measurement slope of the room temperature sample at 5 m/s. If the test for the heated sample at 4 m/s was carried out over 60 minutes, the turbidity measurements would have surpassed the turbidity measurements of room temperature sample at 5 m/s. However, turbidity measurements are not indicative of erosion rate at this time; the slope of the turbidity plot may offer a better representation of erosion rate, as shown in Fig. 42, where the heated sample at 4 m/s resulted in more erosion than the room temperature sample at 5 m/s. Nevertheless, the turbidity measurements of the room temperature sample at 5 m/s were higher than the turbidity measurements of the heated sample at 4 m/s, despite that more erosion occurred in the heated sample.

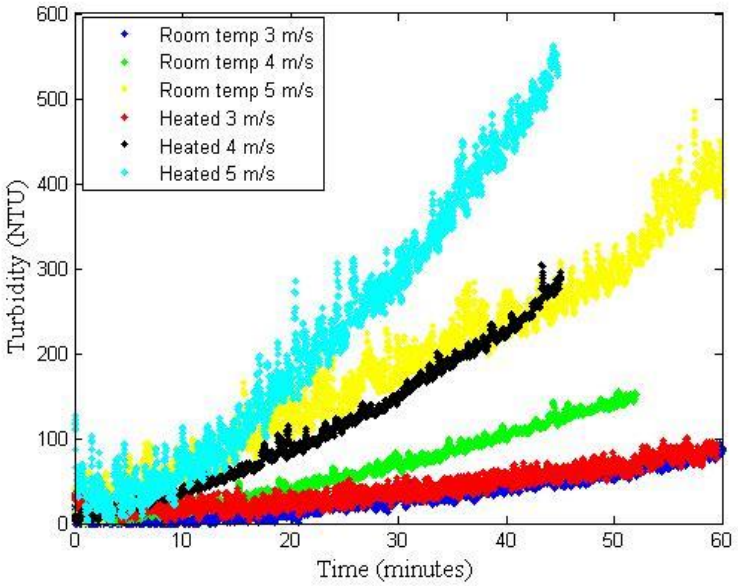

Fig. 42 Comparison of turbidity plots

The slope of the turbidity plot was estimated and presented in Table 7. The estimated slope for heated and room temperature samples tested at flow velocity of 3 m/s were the same and that is thought to be a result of poor sample mixing as the water recirculates through the system. Although there is a slight discrepancy in turbidity values, where the heated sample resulted in higher turbidity values than the room temperature sample, the estimated slopes were equal. However, for faster velocities, 4 and 5 m/s, the estimated turbidity slope seems to agree with measured erosion rates, showing that heated samples tested under flow velocities 4 and 5 m/s resulted in steeper slopes than room temperature samples tested under the same flow velocities.

Table 7 Estimated slope of turbidity plots

Sample's Condition	Flow Velocity (m/s)	Erosion Rate (mm/hour)	Estimated Slope (NTU/minutes)
Heated (32°C)	3	9.5	2.5
Heated (32°C)	4	19	8
Heated (32°C)	5	27	16
Room temperature (21°C)	3	6	2.5
Room temperature (21°C)	4	8	3.5
Room temperature (21°C)	5	12	7

In conclusion, effects of soil temperature on erosion rate revealed that an increase in soil temperature directly increases fine-grained soil erodibility. Effects of increasing water temperature on erosion rate showed a slight increase in erosion rate when the circulating water's temperature was allowed to increase, although the observed difference was not more than 4 mm/hour since the test was initiated with cold water and the temperature was allowed to increase over the duration of the test. The turbidity sensor employed in this study confirmed and compared erosion rates for samples tested under identical velocities. The sensor measured minute differences in erosion rate, as little as 0.5 mm/hour. Also, the slope of the turbidity plot is related to erosion rate for flow velocities greater than 3 m/s.

Chapter 5 - Concluding Remarks

The main objective of this study was to investigate the effects of fine-grained soil temperature on soil erodibility. Grabowski et al. (2011) previously identified temperature as one of the factors that influence erodibility, but prior to this study, a slight increase, between 10 and 20 °C, in fine-grained soil temperature effects on erosion rate were unknown. Effects of water temperature on soil erodibility were also investigated to complement a previous study by Larionov et al. (2014). A turbidity sensor was employed in this study to map soil erosion and compare erosion results of identical samples tested under similar velocities. This section includes a brief summary of sample preparation, conclusions based on testing heated samples, and concluding remarks on the effects of water temperature and turbidity sensor instrumented in this study. Finally, recommendations for future studies are presented.

Samples used in this study were identically prepared to ensure consistent results when tested in the EFA. Kaolin clay was mixed to an optimum moisture content of 29% and compacted to a maximum dry unit weight of 14.23 $kN/m^3 \pm 1$ kN/m^3. Moisture content and maximum dry unit weight were determined by the Standard Proctor test. All soil samples were compacted in a 30.5 cm Shelby tube in one layer to eliminate effects of layering. Seven tests were performed on soil samples in the EFA to ensure consistent results before varying soil temperature in order to study temperature effects on erosion rates. Samples A through D in Table 8 were tested for consistency which shows maximum discrepancy of 3 mm/hour occurred at flow velocity of 4 m/s. Table 8 Summary of all samples tested in the EFA

By employing a custom heating system, soil temperature was successfully brought to and maintained at temperatures above room temperature. A comparison of results of all tests performed on room temperature samples and heated samples revealed a direct relationship

between soil temperature and erosion rates: soil samples at temperatures above room temperature demonstrated greater erosion than soil samples tested at room temperature. For example, sample H-6 was heated to 37 ˚C, when tested under flow velocity of 6 m/s, sample H-6 resulted in erosion rate of 60 mm/hour. By comparison the room temperature sample R-1 resulted in erosion rate of 12 mm/hour when tested under the same velocity of 6 m/s. Therefore, because soil temperature was identified as an important variable in fine-grained soil erosion, engineers should monitor, maintain, and record soil temperatures in their laboratory studies.

This study also confirmed the effects of increasing water temperatures on erosion rates. A room temperature sample was tested as the circulating water temperature was allowed to increase from 16 to 30 °C and the results are compared to results of room temperature samples tested as circulating water temperature was maintained between 16 and 20 °C. A slight difference in erosion rates was observed, although the difference was not significant since the tests conducted were all initiated at approximately equivalent water temperatures. In order to precisely study the effects of water temperature on erosion rates, tests should be initiated and maintained at various water temperatures instead of initiating the test at low water temperatures and allowing the water to warm as energy is being converted. In order to accurately measure soil erosion rates in laboratories, the circulating water temperature should be similar to the water temperature measured in situ.

In this study, a turbidity sensor was instrumented downstream from the test section in order to map soil erosion as it occurred. By measuring light-scattering effects in liquid media, the sensor demonstrated accuracy in measuring minute differences in erosion rates, as low as 0.5 mm/hour. When comparing turbidity plots obtained from the sensor, only similar velocities should be compared. For example, turbidity plots of samples tested at a flow velocity of 2 m/s

should only be compared to samples tested at flow velocities of 2 m/s. Additionally, when engaging the sensor for comparison purposes, only samples of identical composition should be compared with one another since soil samples of different compositions may result in unexpected turbidity measurements. A major advantage of the sensor was its ability to show which sample had eroded more. However, because the sensor measures the concentration of particles in water, it could only be employed when no water was entering or leaving the EFA. Furthermore, the sensor could not be employed in controlled water temperature tests because controlling water temperature was achieved by filling and draining the EFA simultaneously.

Based on findings of this study, researchers conducting laboratory erosion studies on in situ soil samples should test under temperatures that represent in situ conditions. This study also suggests that a storm event of a certain magnitude in warm seasons will cause more erosion and sediment loss than a storm event of the same magnitude in cold seasons. Table 8 summarizes results of all tests performed in this study.

Table 8 Summary of all samples tested in the EFA

Sample ID	Soil Temperature (°C)	Dry Unit Weight (kN/m^3)	Water Content (%)	1 m/s (mm/hr)	2 m/s (mm/hr)	3 m/s (mm/hr)	4 m/s (mm/hr)	5 m/s (mm/hr)	6 m/s (mm/hr)
Consistent Samples									
A	21	14.66	29	NA	NA	4	10	NA	NA
B	21	14.8	29.5	NA	NA	4	9	11	14
C	21	14.7	29.3	NA	NA	5	10	11	13
C-1	21	14.7	29.3	NA	NA	4	9	11	14
C-2	21	14.7	29.3	NA	NA	4	8	NA	NA
D	21	14.74	29	NA	NA	4	7	NA	NA
D-1	21	14.74	29	NA	NA	3	7	NA	NA
Soil Temperature									
H-1	30	14.63	29.19	0	3	9	17	NA	NA
H-2	32	14.64	29.33	0	4	9.5	19	27	NA
H-3	34	14.69	29.1	0	3	9	15	24	NA
H-4	34	14.76	29	0	3	12	21	NA	NA
H-5	35	14.63	29.19	0	3	9	18	42	NA
H-6	37	14.64	29.33	0	3	9	15	24	60
R-1	21	14.62	29.04	NA	NA	NA	6	9	12
R-2	21	14.62	29.04	1	2.5	6	8	12	15
R-3	21	14.8	28	0	0	9	12	NA	NA
R-4	21	14.7	29.3	0	1	5	10	NA	NA
R-5	21	14.7	29.3	0	0	4	9	11	13
R-6	21	14.7	29.3	0	1	4	8	11	14
R-7	21	14.66	29	NA	0	NA	6	12	NA
R-8	21	14.31	NA	NA	NA	NA	6	12	NA
Water Temperature									
Uncontrolled	21	14.62	29.04	1	2.5	6	8	12	NA
Controlled Test1	21	14.6	29.8	0	2	4	6	9	NA
Controlled Test2	21	14.56	28.5	0	2	4	5	8	NA

Future Work

This study illustrated the effects of above-room-temperature samples on fine-grained soil erosion rate. However, the effects of below-room-temperature samples on the erosion rate of fine-grained soil remains unknown. Therefore, future studies should investigate the effects of below-room-temperature samples on fine-grained soil erodibility. Because the earth experiences seasonal variations every year, cold seasons followed by warm seasons, another recommendation for future study is to investigate the effects of cyclic cooling and heating soil samples on fine-grained soil erodibility. An increase in soil temperature has been shown to increase erosion rates in fine-grained soils, but how small of a difference in soil temperature impacts fine-grained soil erodibility is unknown and should be investigated in future studies. The final recommendation for future studies is to instrument an additional turbidity sensor upstream from the test section where the difference in turbidity measurements can be associated with how much erosion occurs. The additional sensor would allow both sensors to be employed on controlled water tests.

References

American Society of Testing and Materials. (2012). "Standard Test Methods for Laboratory Compaction Characteristics of Soil using Standard Effort." *Astm,* D698-12.

American Society of Testing and Materials. (2007). "Standard Test Method for Particle-Size Analysis of Soils." *Astm,* D422-63.

Amos, C. L., Li, M. Z., Sutherland, T. F. (1998). "The Contribution of Ballistic Momentum Flux to the Erosion of Cohesive Beds by Flowing Water." *J. Coast. Res.,* 14(2), 564-569.

Briaud, J. -., Chen, H. -., Li, Y., Nurtjahyo, P. (2004). "SRICOS-EFA Method for Complex Piers in Fine-Grained Soils." *Journal of Geotechnical and Geoenvironmental Engineering,* 130(11), 1180-1191.

Briaud, J. L., Ting, F. C. K., Chen, H. C., Cao, Y., Han, S. W., Kwak, K. W. (2001). "Erosion Function Apparatus for Scour Rate Predictions." *J. Geotech. Geoenviron. Eng.,* 127(2), 105-113.

Briaud, J. -. (2008). "Case Histories in Soil and Rock Erosion: Woodrow Wilson Bridge, Brazos River Meander, Normandy Cliffs, and New Orleans Levees." *J. Geotech. Geoenviron. Eng.,* 134(10), 1425-1447.

Briaud, J. -. (2006). "Bridge Scour." *Geotech News,* 24(3), 54-56.

Briaud, J. -., Ting, F. C. K., Chen, H. C., Gudavalli, R., Perugu, S., Wei, G. (1999). "SRICOS: Prediction of Scour Rate in Cohesive Soils at Bridge Piers." *J. Geotech. Geoenviron. Eng.,* 125(4), 237-246.

Crowley, R. W., Bloomquist, D., Robeck, C. (2012). "Description of erosion rate testing devices and correlations between rock erosion and cohesion." *Proc., International Conference on Scour and Erosion,* ICSE6, Paris, 205.

Crowley, R. W., Bloomquist, D. B., Shah, F. D., Holst, C. M. (2012). "The Sediment Erosion Rate Flume (SERF): A New Testing Device for Measuring Soil Erosion Rate and Shear Stress." *Geotech Test J,* 35(4).

Davies-Colley, R. J., and Smith, D. G. (2001). "Turbidity, Suspended Sediment, and Water Clarity: A Review." *Jawra,* 37(5), 1085-1101.

Debnath, K., Nikora, V., Elliott, A. (2007). "Stream Bank Erosion: In Situ Flume Tests." *J. Irrig. Drain. Eng.,* 133(3), 256-264.

Downing, J. (2008). *Comparison of Suspended Solids Concentration (SSC) and Turbidity,* Campbell Scientific, Inc, Logan, UT.

Gebert, J., Köthe, H., Grönggröft, A. (2006). "Prognosis of Methane Formation by River Sediments." *Journal of Soils and Sediments,* 6(2), 75-83.

Gerbersdorf, S. U., Jancke, T., Westrich, B. (2007). "Sediment Properties for Assessing the Erosion Risk of Contaminated Riverine Sites. A Comprehensive Approach to Evaluate Sediment Properties and their Covariance Patterns Over Depth in Relation to Erosion Resistance - First Investigations in Natural Sediments at Three Contaminated Reservoirs." *Journal of Soils and Sediments,* 7(1), 25-35.

Grabowski, R. C., Droppo, I. G., Wharton, G. (2011). "Erodibility of Cohesive Sediment: The Importance of Sediment Properties." *Earth-Sci. Rev.,* 105(3-4), 101-120.

Hanson, G. J., and Cook, K. R. (2004). "Apparatus, Test Procedures, and Analytical Methods to Measure Soil Erodibility in Situ." *Appl. Eng. Agric.,* 20(4), 455-462.

Hanson, G. J. (1991). "Development of a Jet Index to Characterize Erosion Resistance of Soils in Earthen Spillways." *Trans. ASAE,* 34(5), 2015-2020.

Inbar, A., Lado, M., Sternberg, M., Tenau, H., Ben-Hur, M. (2014). "Forest Fire Effects on Soil Chemical and Physicochemical Properties, Infiltration, Runoff, and Erosion in a Semiarid Mediterranean Region." *Geoderma,* 221-222, 131-138.

Jepsen, R., Roberts, J., Lick, W. (1997). "Effects of Bulk Density on Sediment Erosion Rates." *Water Air Soil Pollut.,* 99(1-4), 21-31.

Johnson, P. A. (2015). "Bridge scour and stream stability." <http://www.personal.psu.edu/faculty/p/a/paj6/Research.html> (10/30, 2015).

Larionov, G. A., Bushueva, O. G., Dobrovol'skaya, N. G., Kiryukhina, Z. P., Krasnov, S. F., Litvin, L. F. (2014). "Effect of the Water Temperature and Soil Moisture on the Erodibility of Chernozem Samples: A Model Experiment." *Eurasian Soil Sci.,* 47(7), 734-739.

Leeder, M. R. (1999). *Sedimentology and Sedimentary Basins: From Turbulance to Tectonics,* Blackwell, Oxford, 592.

McNeil, J., Taylor, C., Lick, W. (1996). "Measurements of Erosion of Undisturbed Bottom Sediments with Depth." *J. Hydraul. Eng.,* 122(6), 316-324.

Moore, W. L., and Masch, F. D. J. (1962). "Experiments on the Scour Resistance of Cohesive Sediments." *Journal of Geophysical Research,* 67(4), 1437-1446.

Munson, B. R., Young, D. F., Okiishi, T. H. (2002). *Fundamentals of Fluid Mechanics,* Wiley, New York.

Partheniades, E. (1965). "Erosion and Deposition of Cohesive Soils." *Journal of the Hydraulics Division,* 91(1), 105-139.

Ravens, T. M. (2007). "Comparison of Two Techniques to Measure Sediment Erodibility in the Fox River, Wisconsin." *J. Hydraul. Eng.,* 133(1), 111-115.

Roberts, J., Jepsen, R., Gotthard, D., Lick, W. (1998). "Effects of Particle Size and Bulk Density on Erosion of Quartz Particles." *J. Hydraul. Eng.,* 124(12), 1261-1267.

Roberts, J. D., Jepsen, R. A., James, S. C. (2003). "Measurements of Sediment Erosion and Transport with the Adjustable Shear Stress Erosion and Transport Flume." *J. Hydraul. Eng.,* 129(11), 862-871.

Sanders, I. A., Heppell, C. M., Cotton, J. A., Wharton, G., Hildrew, A. G., Flowers, E. J., Trimmer, M. (2007). "Emission of Methane from Chalk Streams has Potential Implications for Agricultural Practices." *Freshwat. Biol.,* 52(6), 1176-1186.

Schaaff, E., Grenz, C., Pinazo, C., Lansard, B. (2006). "Field and Laboratory Measurements of Sediment Erodibility: A Comparison." *J. Sea Res.,* 55(1), 30-42.

Sheppard, D. M., and Bloomquist, D. (2005). *Design and Construction of Apparatus for Measuring Rate of Water Erosion of Sediments,* Florida Department of Transportation, Tallahassee, FL.

Trenberth, K. E. (2011). "Changes in Precipitation with Climate Change." *Climate Research,* 47(1), 123.

Winterwerp, J. C., and van Kesteren, W. G. M. (2004). *Introduction to the Physics of Cohesive Sediment in the Marine Environment,* Elsevier, Amsterdam, 576.